Front. Environ. Sci. Eng. 2024, 18(7): 86
https://doi.org/10.1007/s11783-024-1846-x

REVIEW ARTICLE

A review on Bi_2WO_6-based photocatalysts synthesis, modification, and applications in environmental remediation, life medical, and clean energy

Wei Mao[1,2], Xuewu Shen[1,2], Lixun Zhang (✉)[1,2], Yang Liu[1,2], Zehao Liu[1,2], Yuntao Guan (✉)[1,2]

1 Guangdong Provincial Engineering Technology Research Center for Urban Water Cycle and Water Environment Safety, Tsinghua Shenzhen International Graduate School, Tsinghua University, Shenzhen 518055, China
2 State Environmental Protection Key Laboratory of Microorganism Application and Risk Control, School of Environment, Tsinghua University, Beijing 100084, China

HIGHLIGHTS

- Recent progress of bismuth tungstate (Bi_2WO_6) as photocatalyst was summarized.
- The review reported the fabrication and modification of Bi_2WO_6-based materials.
- Bi_2WO_6-based photocatalysts have been widely used in multiple areas.
- Future perspectives on the use of Bi_2WO_6-based photocatalysts were discussed.

ARTICLE INFO

Article history:
Received 10 January 2024
Revised 13 March 2024
Accepted 13 March 2024
Available online 11 April 2024

Keywords:
Bismuth tungstate
Synthesis and modification
Photocatalytic application
Environmental remediation
Clean energy
Medical science

GRAPHIC ABSTRACT

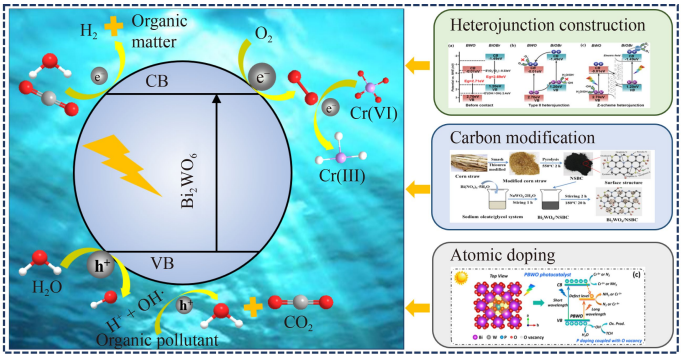

ABSTRACT

Photocatalysis has emerged a promising strategy to remedy the current energy and environmental crisis due to its ability to directly convert clean solar energy into chemical energy. Bismuth tungstate (Bi_2WO_6) has been shown to be an excellent visible light response, a well-defined perovskite crystal structure, and an abundance of oxygen atoms (providing efficient channels for photogenerated carrier transfer) due to their suitable band gap, effective electron migration and separation, making them ideal photocatalysts. It has been extensively applied as photocatalyst in aspects including pollutant removal, carbon dioxide reduction, solar hydrogen production, ammonia synthesis by nitrogen photocatalytic reduction, and cancer therapy. In this review, the fabrication and application of Bi_2WO_6 in photocatalysis were comprehensively discussed. The photocatalytic properties of Bi_2WO_6-based materials were significantly enhanced by carbon modification, the construction of heterojunctions, and the atom doping to improve the photogenerated carrier migration rate, the number of surface active sites, and the photoexcitation ability of the composites. In addition, the potential development directions and the existing challenges to improve the photocatalytic performance of Bi_2WO_6-based materials were discussed.

1 Introduction

Currently, human beings are facing a variety of problems including environment pollution, global climate change, and energy consumption. The inexhaustible renewable energy of solar has been widely concerned by numerous researchers. To address the looming problems of environmental pollution and energy shortage, the photocatalysis technology has been recognized as a promising treatment method to convert solar energy into chemical energy

✉ Corresponding authors
E-mails: lixunz@sz.tsinghua.edu.cn (L. Zhang);
guanyt@tsinghua.edu.cn (Y. Guan)

(Fehr et al., 2023). By modifying photocatalyst, photocatalysis technology which is a potential technology for green development can effectively enhance solar energy utilization and pollutant removal, which is a potential technology for green development (Mao et al., 2022c; Shi et al., 2023). Photocatalysis technology mainly aims to form electrons and holes in the catalyst under light excitation and produce a series of active substances with high REDOX potential, which may destroy the internal chemical bonds of organic or inorganic pollutants in the environment through REDOX reaction degrade pollutants (Huang et al., 2019; Li et al., 2020a). After decades of research, photocatalysis has achieved significant breakthroughs in some crucial areas including the development and research of catalyst mechanism, removal of organic pollutants, water cracking to produce hydrogen, detoxification of highly toxic inorganic, as well as reduction of carbon dioxide (CO_2) into fuel (Liu et al., 2022; 2023; Monticelli et al., 2023). In the development and application of semiconductor photocatalysts, titanium dioxide (TiO_2) is one of the most investigated photocatalysts due to its non-toxicity, good stability, and low price (Cao et al., 2023; Haider et al., 2023). However, TiO_2 is not very responsive to visible light, seriously restricting its practical application. Therefore, it is of great necessity to develop a photocatalyst with high visible light responsive ability to enhance the utilization rate of solar energy.

Nowadays, numerous researchers have concentrated on the preparation of photocatalysts with narrow band gap and high-efficiency photogenerated carrier separation. Previous reports indicate that bismuth materials have promising applications in the field of photocatalysis due to their strong visible-light corresponding ability (Feng et al., 2022). Bismuth tungstate (Bi_2WO_6) is a kind of perovskite semiconductor material, which is characterized by good visible light excitation activity and suitable band gap energy (2.8 eV). Compared with other photocatalysts including $BiVO_4$ (Wang et al., 2022), CuO (Cao et al., 2021), MoS_2 (Lin et al., 2023), g-C_3N_4 (Mao et al., 2018; Wang et al., 2021a), CeO_2 (Huang et al., 2016b; Ye et al., 2019; Bai et al., 2020), and CuS (Mao et al., 2021b), Bi_2WO_6 not only effectively lowers the rapid recombination of photogenerated carriers, but also exhibits extreme stability, low environmental toxicity, and corrosive characteristic during the process of actual environmental application (Cao et al., 2021; Wang et al., 2022). Wang et al. extensively investigated the synthetic methods and the modification measures of Bi_2WO_6 to improve the photocatalytic performance of the composite (Wang et al., 2015; 2019; 2020b). To improve the photocatalytic performance of Bi_2WO_6 in environmental applications, Jiang et al. focused on enhancing the visible light response of Bi_2WO_6 by carbon doping modification (Jiang et al., 2023). The doping of nonmetallic elements, such as carbon, nitrogen, phosphorus, and sulfur, may form a strong electric field into the interface and show a more efficient photogenerated carrier transfer (Guo et al., 2023). Although numerous researches have already concentrated on the photocatalytic properties of Bi_2WO_6 and its application in environmental remediation (Fig. 1), its comprehensive application in the fields of environmental remediation, medicine and clean energy has not yet been discussed. Therefore, reviewing and summarizing the current research results will exert a strong role in guiding the future synthesis of high-performance Bi_2WO_6-based photocatalytic composites. In this study, the photocatalytic properties and mechanism of Bi_2WO_6-based materials were also introduced. The photocatalytic performance of Bi_2WO_6-based material and its application in actual water were discussed. Finally, the potential research directions and applications of Bi_2WO_6-based materials in the future were prospected.

2 Synthesis, structure, and characteristics of Bi_2WO_6

Recently, different preparation methods have been employed to synthesize Bi_2WO_6 nanoparticles to form different microstructure, including nano-flowers, hierarchical microsphere, nano-sheets, microspheres, nanorods, nano-plates, and nano-cuboids (Zhang et al., 2019; Wei et al., 2020; Orimolade et al., 2021). The morphology of Bi_2WO_6 influencing the photocatalytic abilities mainly is dependent on the synthesis methods (Meng et al., 2017). Up to now, the preparation methods of Bi_2WO_6 include hydrothermal synthesis, solvothermal, calcination, and electrodeposition (Hu et al., 2019; Wang et al., 2021b; 2023a). The preparation method tremendously determines the crystal lattice and morphology of Bi_2WO_6. For example, the hydrothermal reaction generally facilitates the formation of nano-like structure, while the calcination method usually results in an agglomerate structure, which

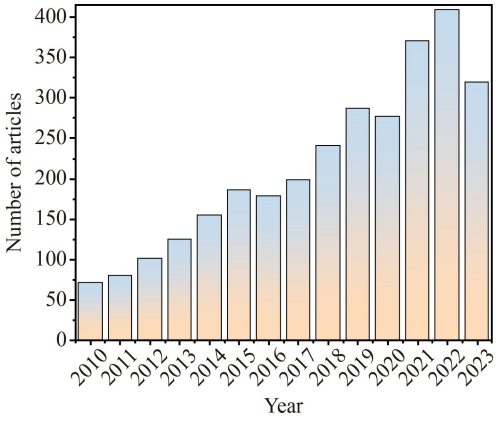

Fig. 1 Graph showing the number of papers published annually on photocatalysis field by Bi_2WO_6 composites (Data extracted from Web of Science Database).

may influence the photocatalytic performance by adjusting the number of active sites on the surface of the composite and the adsorption capacity of the treated object. Due to the large and stable specific surface area of the obtained composite, the hydrothermal/solvothermal method has been widely used to synthesize Bi_2WO_6 (Table 1).

In many cases, the lattice and surface morphology of Bi_2WO_6 were regulated by adding surfactants, choosing different solvents, as well as controlling pH and temperature of the reaction system during synthesis. In the study performed by Mao et al. (2018), Bi_2WO_6 nanoparticles were prepared by adding sodium oleate with hydrothermal reaction (Fig. 2(a)). Similarly, Yuan et al. (2019) fine-tuned the gas-sensitive properties and structure of Bi_2WO_6 nanoparticles during hydrothermal preparation by the addition of hexadecyl trimethyl ammonium chloride (CTAC) (Fig. 2(b)). Ultra-thin nanosheets with a thickness of 6.5 nm were reassembled into a uniform three-dimensional layered nanoflower structures. It was found that the addition sequence of bismuth nitrate ($Bi(NO_3)_3·5H_2O$) and sodium tungstate made an impact on the synthesis of Bi_2WO_6, mainly due to the strong hydrolysis property of $Bi(NO_3)_3·5H_2O$. Moreover, the addition of CTAC would directly affect the assembly of Bi_2WO_6, and numerous atoms were generated at the crystal-amorphous boundary of the composite with excessive CATC. In the meanwhile, a three-dimensional microsphere of Bi_2WO_6 was effectively prepared by sol-gel hydrothermal method with EDTC as the reaction solvent (Liu et al., 2014). A nanoparticle of Bi_2WO_6 was synthesized by microwave-assisted pyrolysis in sequence (Phu et al., 2015). Zhao et al. (2018a) found that the Bi_2WO_6 exhibited a nanoflower morphology in a synthetic environment with a pH of 1–7, while the nanoplate structures dominated when the reaction liquid pH was 9–11 (Zhao et al., 2018a). Specifically, the structure of Bi_2WO_6 gradually changed from the nanoflowers, nodular, rod-like, and irregular shapes with the pH value of the reaction system ranging from 1 to 11, respectively. Bi_2WO_6 with a nanoflower structure exhibited the highest photocatalytic removal ability of ceftriaxone sodium, possibly due to the large specific surface area contributing to light capture. Moreover, microdisk, porous nanoplates, and ultrathin monolayer structures of Bi_2WO_6 can be synthesized by the assistance of acetic acid, egg white proteins (albumin), or the assistance of a cetyltrimethylammonium bromide, respectively (Yi et al., 2019). It is mainly caused by the fact that the addition of surfactants can lower the band gap energy of Bi_2WO_6, and hinder the accumulation of monolayer through coulomb repulsion, which may result in the production of unsaturated coordination and the active sites.

3 Modification of Bi_2WO_6

The intrinsic factors of influencing the photocatalytic performance of Bi_2WO_6 include the light absorption range, photoelectron migration rate, photogenerated carrier separation and recombination efficiency, band gap width, and the number of surface active sites (Bai et al., 2021; Zhang et al., 2023). Nevertheless, it is difficult for Bi_2WO_6 to fully satisfy the needs of photocatalysis, primarily due to its low visible light response, relatively wide band gap, and fast photogenerated electron-hole recombination. Therefore, it is essential to improve the photocatalytic performance of Bi_2WO_6 using a series of modification methods, including the construction of p-n heterojunction, carbon load, and atomic doping.

3.1 The construction of semiconductor heterojunction

The construction of semiconductor heterojunction is an effective modification method for Bi_2WO_6 enhancing the

Table 1 Summary of synthesis and photocatalytic properties of Bi_2WO_6

Photocatalyst	Synthesis method	Morphology	Specific surface area (m^2/g)	Contaminant	Removal efficiency	Photocatalysis condition	Ref.
Bi_2WO_6	Hydrothermal	Nanoflowers	26.154	Ceftriaxone sodium	70.18%	C_0 = 10 mg/L; t = 240 min; dosage = 1 g/L; LS: 300 W Xenon lamp	Zhao et al. (2018b)
Bi_2WO_6	Solvothermal	Nanosheets and microspheres	–	Rhodamine B	97%	C_0 = 10 mg/L; t = 180 min; dosage = 0.2 g/L; LS: 420 W Xenon lamp	Ma et al. (2016)
Bi_2WO_6-g-C_3N_4	Microwave hydrothermal	Nanosheets	103.01	Atrazine	100%	C_0 = 10 mg/L; t = 60 min; dosage = 0.8 g/L; LS: 500 W Xenon lamp	Yang et al. (2023a)
BPQD/BWO	Hydrothermal	Porous hollow spheres	67.03	Amoxicillin	94.5%	C_0 = 20 mg/L; t = 60 min; dosage = 0.25 g/L; LS: 300 W Xenon lamp	Chen et al. (2023)
In_2S_3/Bi_2WO_6	Hydrothermal	Chrysanthemum -like	64.8	Tetracycline hydrochloride	96%	C_0 = 20 mg/L; t = 120 min; dosage = 1 g/L; LS: 300 W Xenon lamp	He et al. (2022)
Bi_2S_3-Bi_2WO_6	Hydrothermal	Nanorods	–	Carbamazepine	92%	C_0 = 5 mg/L; t = 30 min; dosage = 0.5 g/L; LS: 100 W Xenon lamp	Cheng et al. (2022)
CQDs/Bi_2WO_6	Hydrothermal	Petal-like	35.56	Tetracycline	89%	C_0 = 20 mg/L; t = 40 min; dosage = 0.6 g/L; LS: 300 W Xenon lamp	Ren et al. (2023)
PPy/BWO	Solvothermal-calcining	Flower spherical	–	Cr(VI)	99.7%	C_0 = 10 mg/L; t = 30 min; dosage = 0.15 g/L; LS: 300 W Xenon lamp	Song et al. (2022)

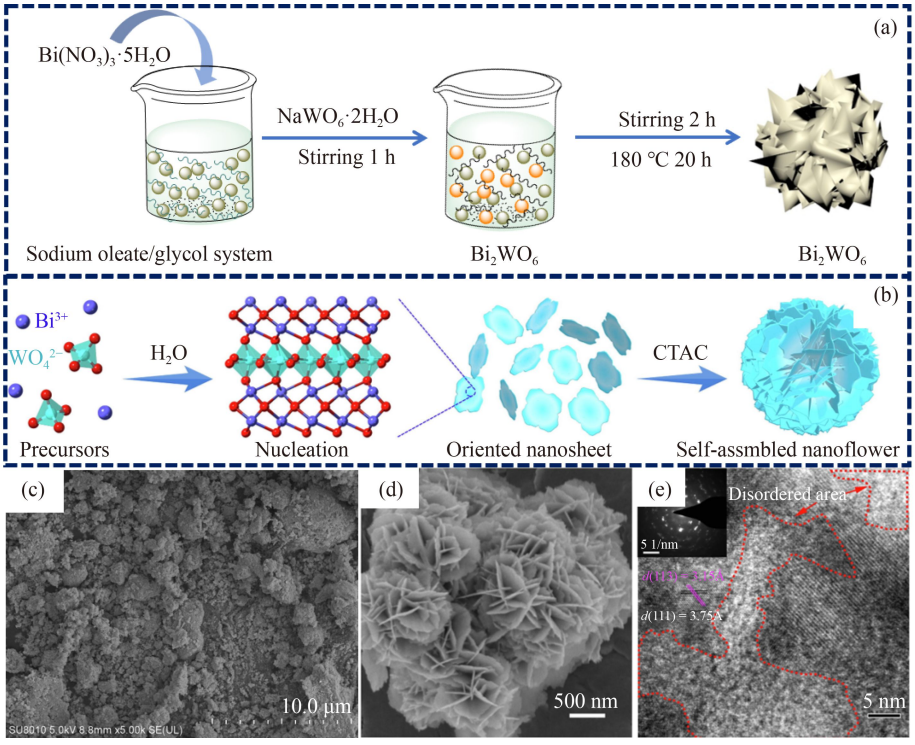

Fig. 2 The synthetic path of Bi_2WO_6 (a and b), (c and d) SEM and (e) HRTEM images of Bi_2WO_6 microstructure. Reprinted from Ref. (Yuan et al., 2019; Mao et al., 2021a) with permission from Elsevier, Chinese Academy of Sciences, and National Natural Science Foundation of China.

photocatalytic carrier separation efficiency and photocatalytic response. Semiconductor p-n heterojunction catalysts are generally formed by two or more P-type and N-type semiconductors closely linked through hydrothermal or other reactions. Meanwhile, the heterojunction interface of composite material promotes the effective separation of photogenerated electrons and holes, which may further enhance the photocatalytic performance. As shown in Fig. 3, n-type semiconductor Bi_2WO_6 and p-type semiconductor $BiFeO_3$ successfully formed p-n heterojunction structure, possibly because of the electron migration from Bi_2WO_6 conduction band to $BiFeO_3$, which may lower and increase electron cloud density of Bi_2WO_6 and $BiFeO_3$, respectively. The photogenerated electrons transfer may induce the internal electric field to further promote the effective separation of photogenerated electron-hole, improving the photocatalytic performance of Bi_2WO_6/$BiFeO_3$. Similarly, through a simple hydrothermal reaction, the p-n heterojunction of Bi_2WO_6/BiOI was constructed (Xiang et al., 2016). XRD and XPS characterization indicate that p-n heterojunction of Bi_2WO_6/CuS has been successfully prepared by sodium oleate glycol system (Figs. 4(a) and 4(b)). The removal mechanism investigation showed that the photogenerated carrier directly oxidizes organic matter and reduces hexavalent chromium (Cr(VI)), as well as realizes the synchronous removal of Cr(VI) and organic matter (Fig. 4(c)).

Although the construction of p-n heterojunction effectively improves the separation and migration of photogenerated carriers, the directional transfer of photogenerated holes to more negative valence bands and electrons to more corrected conduction bands will reduce the redox potentials of photon-induced carrier. Due to the electrostatic repulsion between the same charges, it is prevented from directional migration and enrichment of photogenerated electrons and holes (Chen et al., 2021). To overcome the p-n heterojunction defect, researchers have focused on a Z-type heterojunction similar to plant photosynthesis. During the process of heterogeneous structure construction, Z-type heterojunction can not only realize the efficient separation of photogenerated electrons and holes, but also maintain the original redox properties of photocatalyst.

In the Z-type heterogeneous structure construction, materials with strong conductivity are generally selected as electronic media, including metal atoms (Ni, Cu, Ag, and Au) and conductive carbon-rich materials (carbon nanotubes, graphene, carbon black, carbon fiber, and carbon quantum dots) (Li et al., 2018; Keerthana et al., 2020; Ng et al., 2020; Chen et al., 2021; Zhao et al., 2024a). A carbon quantum dot-decorated BiOBr/Bi_2WO_6 heterojunction was successfully synthesized with a mild hydrothermal method (Fig. 5(a)), and nanoflower-like microspheres were obtained (Figs. 5(b) and 5(c)) (Zhang et al., 2022). Using a series of characterization and

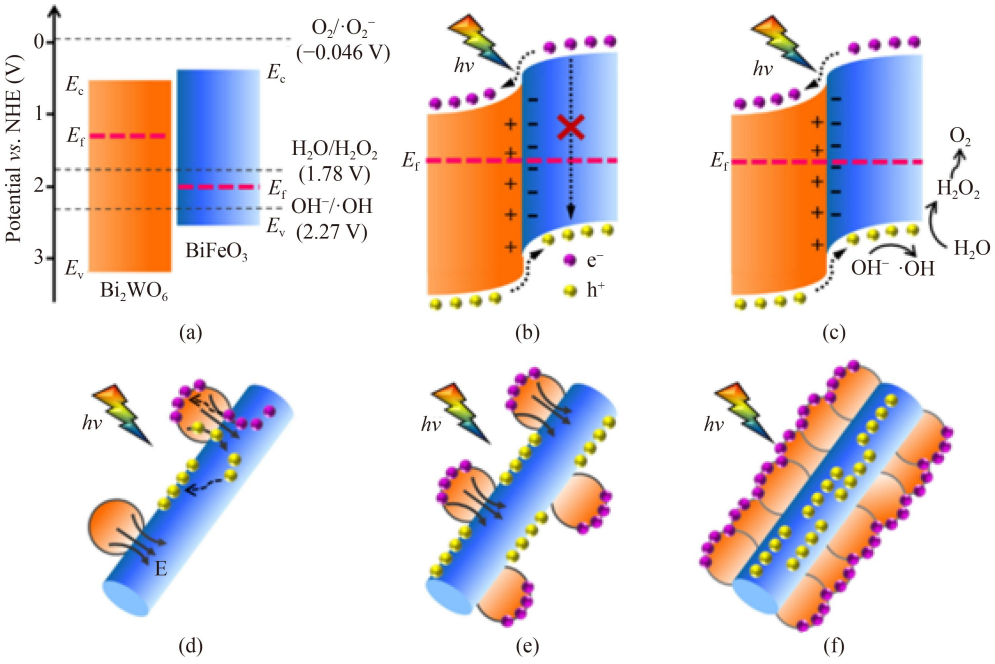

Fig. 3 (a) Semiconductor heterojunction diagram of Bi_2WO_6/$BiFeO_3$; Mechanism of photogenerated charge-separation and -migration (b), and photocatalytic degradation and oxygen evolution in Bi_2WO_6/$BiFeO_3$ (c); Schematic diagram of charge separation and migration in (d) Bi_2WO_6/$BiFeO_3$-1, (e) Bi_2WO_6/$BiFeO_3$-2, and (f) Bi_2WO_6/$BiFeO_3$-3 NFs. Reprinted from Ref. (Tao et al., 2020) with permission from Elsevier.

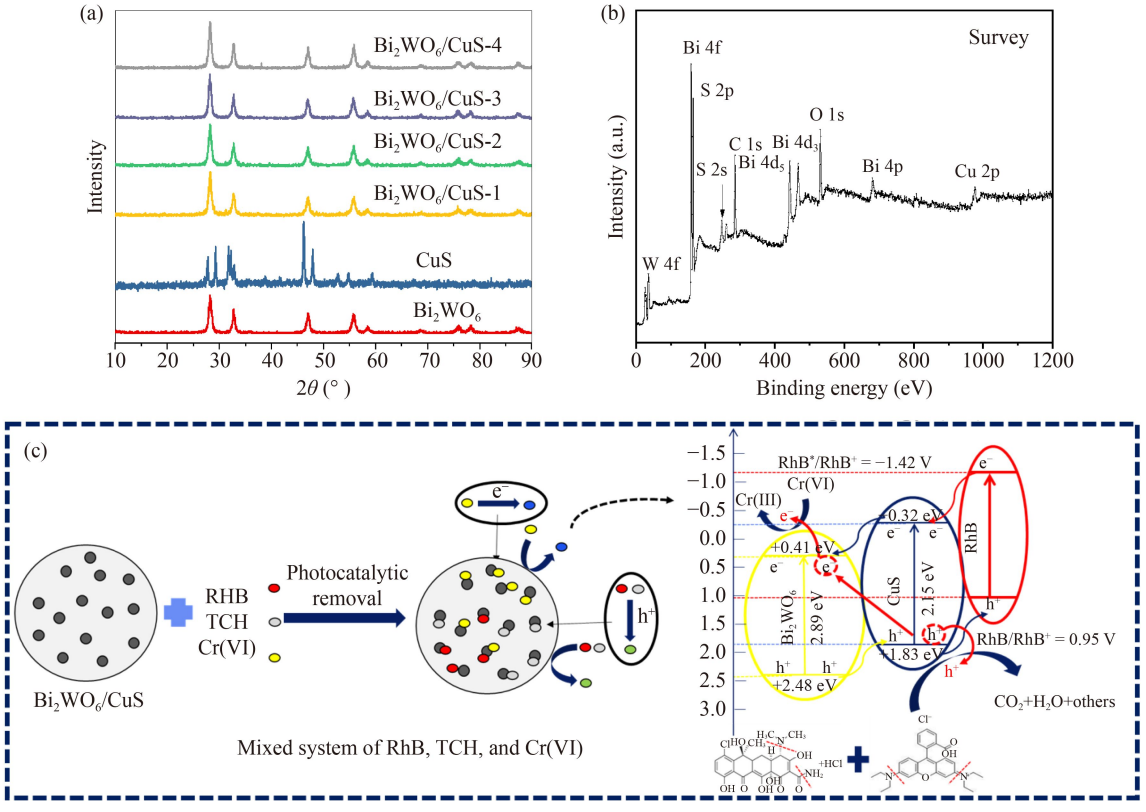

Fig. 4 (a) XRD patterns and (b) XPS spectra of photocatalysts; (c) photocatalytic removal mechanism of mixed RhB, TCH, and Cr(VI). Reprinted from Ref. (Mao et al., 2021b) with permission from Chinese Academy of Engineering and Tsinghua University.

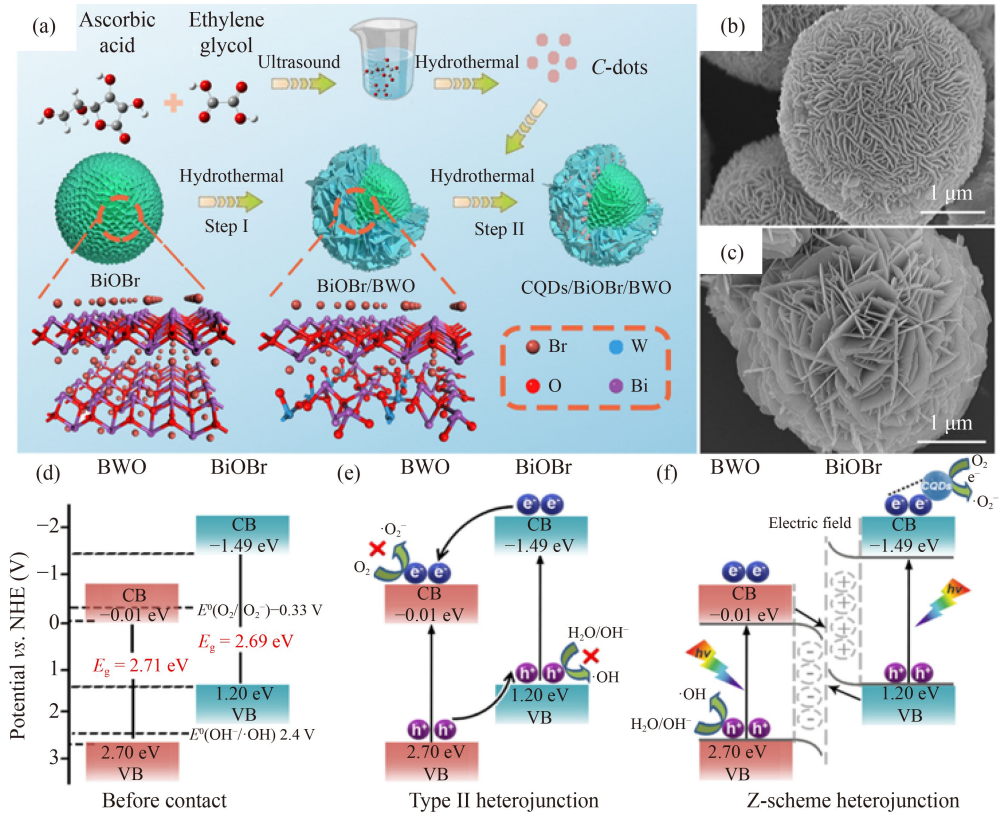

Fig. 5 (a) Schematic representation of the fabrication of CQDs/BiOBr/BWO; SEM images of (b) BiOBr and (c) Bi_2WO_6; (d–f) Charge transfer modes of CQDs/BiOBr/BWO. Reprinted from Ref. (Zhang et al., 2022) with permission from The American Chemical Society.

calculation, the valence and conduction bands of BiOBr were separately +1.20 and −1.49 eV, severally, and those of Bi_2WO_6 were +2.70 and −0.01 eV, respectively (Fig. 5(d)). The photogenerated holes in the valence band of BiOBr can not directly produce hydroxyl radical, and the photoinduced electrons in the conduction band of Bi_2WO_6 can not react with oxygen to produce superoxide radicals (Fig. 5(e)), mainly owing to the failure to reach the standard redox potential of hydroxyl radical and superoxide radical. Therefore, the introduction of carbon quantum dots lowers the band gap of CQDs/BiOBr/BWO by forming Z-type heterojunctions, which will further promote the effective separation of photogenerated carriers and inhibit the recombination of electron and holes (Fig. 5(f)).

3.2 Carbon modification

Carbon-based materials are usually used as carriers of nanometer photocatalysts due to their rich carbon content, special electronic properties, conjugated π structure, and high electrical conductivity, which can act as a strong electron conductor and acceptor to promote electron migration and lower the recombination photogenerated carriers, remarkably improving the photocatalytic performance of the photocatalyst (Mao et al., 2022b; Kang et al., 2023; Yang et al., 2023b). Nowadays, numerous carbon-based materials have been widely used in the field of photocatalysis, including graphitic carbon nitride (g-C_3N_4), biochar (BC), graphene (PG), carbon nano tube, fullerene, and CQDs (Zhou and Zhu, 2012; Mao et al., 2018; Wang et al., 2020b; Li et al., 2021a; Zhao et al., 2022).

As a carbon-based material, g-C_3N_4 has exhibited excellent potential in photocatalysis due to its rich carbon nitrogen, simple preparation process, stable chemical structure, non-toxic and suitable band gap (Li et al., 2020c; Song et al., 2021; Ma et al., 2024). Bi_2WO_6/g-C_3N_4 nanoparticles were prepared by pyrolytic-hydrothermal reaction to realize carbon loading of nanoparticles and form p-n heterojunction interface, which is beneficial for the efficient separation of electrons and holes (Figs. 6(a)–6(d)). Therefore, numerous active substances were produced, probably accelerating the degradation of organic pollutants. Moreover, Bi_2WO_6/g-C_3N_4 based multielement catalysts have been synthesized successively, including BWQ/g-C_3N_4/ATP (Zeng et al., 2022), SnTCPP/g-C_3N_4/Bi_2WO_6 (He et al., 2020), Bi_2WO_6/g-C_3N_4/CeO_2 (Bai et al., 2020), Bi_2WO_6/g-C_3N_4/$BiFeO_3$, and Bi_2WO_6/CuS/g-C_3N_4 (Bai et al., 2021). In addition, they can further increase the number of active sites and facilitate the separation of

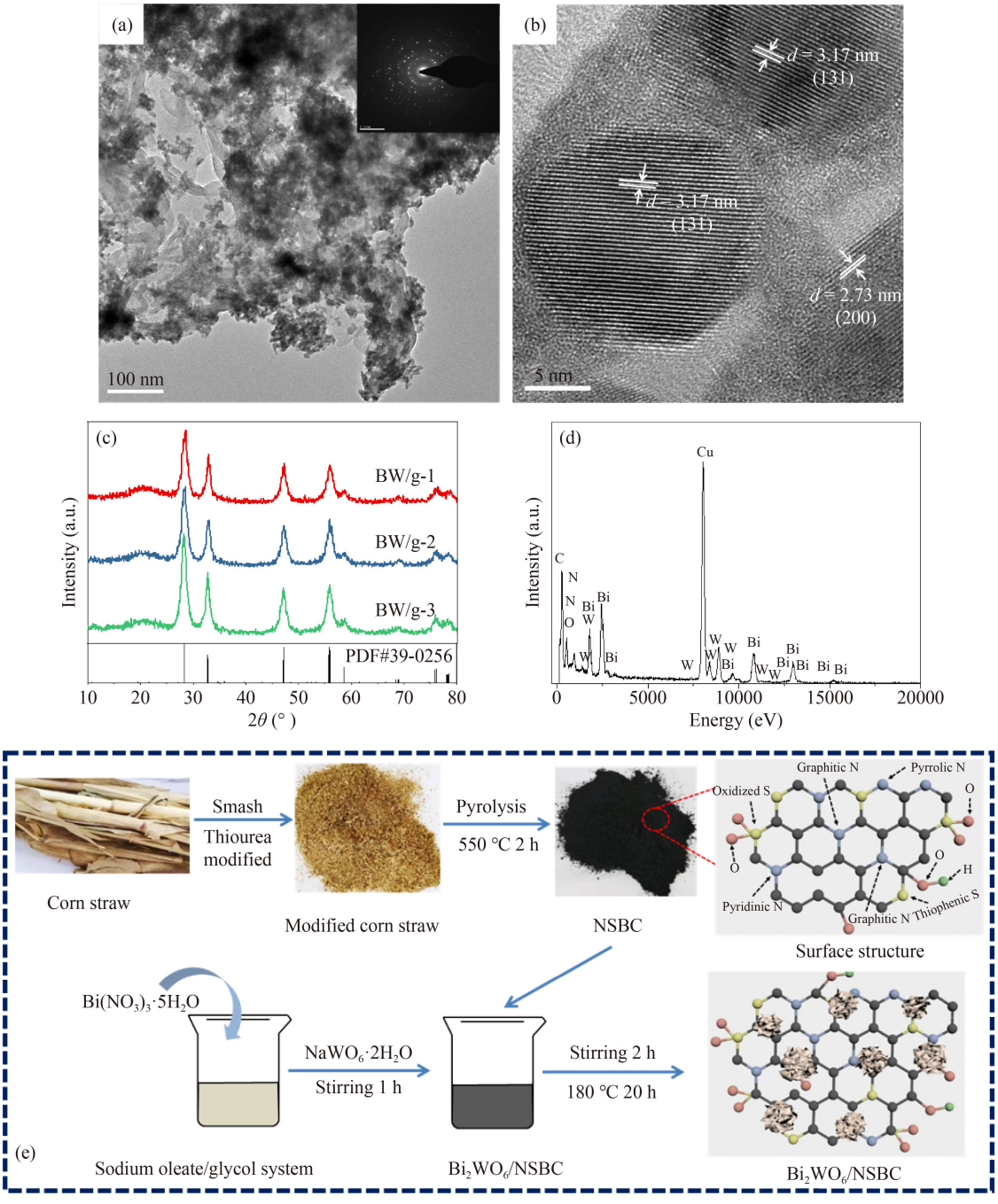

Fig. 6 SEM images of (a)–(b) Bi_2WO_6/g-C_3N_4; (c) XRD patterns and (d) HRTEM micrographs of Bi_2WO_6/g-C_3N_4; (e) Preparation flowchart of the fabrication of Bi_2WO_6/NSBC. Reprinted from Ref. (Mao et al., 2018; Mao et al., 2021a) with permission from Elsevier and SpringerLink.

photogenerated electrons from holes because of the formation of multiple internal electric fields at the heterojunction interface.

BC is a stable, carbon-rich, insoluble, porous, and fluffy substance formed by pyrolysis of biomass at varying temperatures under hypoxic or anaerobic conditions (Kochanek et al., 2022; Monisha et al., 2022). BC is of great interest due to its large specific surface area and wide range of raw materials, including agricultural waste (including peanut shell, pomelo peel, cotton straw, corn straw and animal manure), industrial organic waste, garden waste, and urban sludge (Osman et al., 2022). Therefore, BC has been chosen as the base material to modify Bi_2WO_6, which can enhance the adsorption and photocatalytic properties of the composite. Wang et al. modified BC by nitrogen doping and then loaded Bi_2WO_6 nanoparticles onto the porous carbon skeleton (BW/N-B) (Wang et al., 2020b). Due to the

improved photoelectron migration efficiency and visible light response, the BW/N-B showed an extremely strong photocatalytic performance for the removal of RhB and Cr(VI). Moreover, N-doped BC has been shown to effectively improve the photocatalytic performance of Bi_2WO_6, possibly due to accelerated electron transfer through C-N bonds. To further improve the catalytic performance of Bi_2WO_6, N and S co-doped BC (NSBC) was prepared to disperse Bi_2WO_6. As displayed in Figs. 7(a)–7(c), BC has a large specific surface area and Bi_2WO_6 nano-flowers were successfully loaded onto NSBC by hydrothermal reaction. The structure composition and chemical bond of elements of Bi_2WO_6 were not significantly changed after BC dispersion (Figs. 7(d)–7(g)). Interestingly, photocurrent and electron hole separation rate were significantly increased by NSBC (Figs. 7(h) and 7(i)), probably due to the presence of graphite N, pyridine N, thiophene S, and oxidized S, providing numerous active sites, promoting electron migration, and improving the adsorption of pollutants.

PG is usually used to construct photocatalytic materials due to its outstanding properties including stable chemical structure, fast carrier migration rate, and large specific surface area (Torres-Pinto et al., 2021). Cui et al. (2021) has successfully synthesized GQDs/BWO microspheres via hydrothermal reactions. The results showed that 10 GQDs/BWO had the best photocatalytic ability for degradation of nitrogen oxide (NO), and the conversion of NO by GQDs/BWO was 3.84 times higher than that by pure Bi_2WO_6, possibly owing to the excellent photogenerated electron transfer performance of GQDs (Cui et al., 2021). Additionally, Bi_2WO_6@GNRs nanocomposites were prepared by microwave assisted hydrothermal method, which not only had the excellent electron migration properties, but also exhibited an extremely strong sensing performance (Rajaji et al., 2018).

CQDs have attracted great attention due to its rich carbon content, non-toxicity, and strong photoresponse ability. Qian et al. combined highly stable CQDs with Bi_2WO_6 to enhance the photocatalytic oxidation of gaseous volatile organic compounds (VOCs) (Qian et al., 2016). CQDs/Bi_2WO_6 exhibited the absorption edge of visible light migration and promoted photogenerated carrier transfer, thus achieving efficient photocatalytic

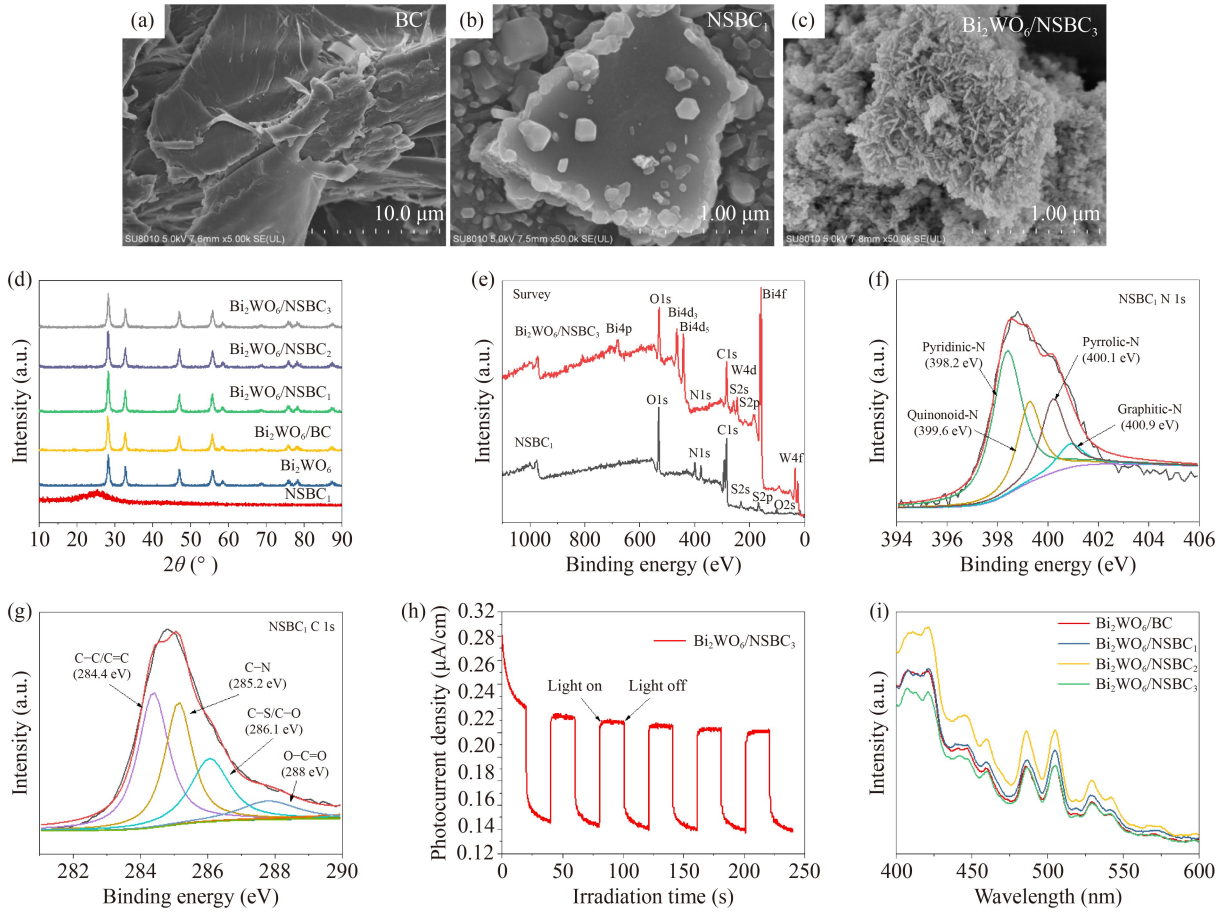

Fig. 7 SEM images of (a) BC, (b) $NSBC_1$, (c) $Bi_2WO_6/NSBC_3$; (d) XRD patterns of the different samples; (e) XPS survey scan, (f) N 1s, (g) C 1s of $NSBC_1$; (h) Transient photocurrent responses and (i) PL spectra of synthesized photocatalysts. Reprinted from Ref. (Mao et al., 2021a) with permission from Elsevier.

oxidation of toluene and acetone under both light and UV-light irradiation. Similarly, CQDs/Bi_2WO_6 was synthesized via *in situ* hydrothermal reaction, and demonstrated that the S-scheme heterojunction interface was connected by Bi-O-C bonds, providing an atomic-level interface channel for promoting photogenerated carrier migration (Ren et al., 2023). To investigate the interface mechanism of CQDs/m-Bi_2WO_6 from the microscopic level, density functional theory (DFT) calculation was employed to investigate the electronic properties of the interface structures (Wang et al., 2018a). As depicted in Figs. 8(a)–8(c), in the interface, photogenerated electrons were accumulated in the CQDs region, while photoinduced holes were enriched in the Bi_2WO_6 region, primarily caused by the VB-edge hybridization and complementary conduction between CQDs and Bi_2WO_6. Meanwhile, CQDs can absorb near-infrared light (400–750 nm) to stimulate Bi_2WO_6 to form hole/electron pairs, and as an electron storage to capture photogenerated electrons emitted by Bi_2WO_6, suppressing electron and hole recombination (Figs. 8(d) and 8(e)). In summary, the modification of CQDs enhanced the photocatalytic removal of organic pollutants under visible light and infrared irradiation.

3.3 Atomic doping

Atomic doping can regulate the lattice of Bi_2WO_6, cause partial defects, improve the efficiency of electron and hole separation, and expand the absorption range of light. Atomic doping is categorized into nonmetallic (P, S, N, F, etc.) and metallic (Ag, Mo, Ce, Cd, Fe, etc.) element doping (Liu et al., 2021a).

The photocatalytic performance of the composites is positively influenced by nonmetallic element doping. Photocatalytic performance of S doped-g-C_3N_4/Bi_2WO_6 was explored by an ultrasonic approach (Murugan et al., 2021). The composite with 3 wt% S doping exhibits the highest photoelectric water oxidation performance, possibly due to the low charge recombination rate by forming heterostructure. Meanwhile, a novel N-CQDs/Bi_2WO_6 was also successfully constructed (Zhang et al., 2018b). Obviously, the photocatalysis and mineralization efficiency of N-CQDs/Bi_2WO_6 were significantly improved with nearly 97% (25 min) and 86.37% (90 min) removal of tetracycline, respectively. This was caused by the acceleration of charge transfer and improvement of molecular oxygen activation ability. Wang et al. (2020a) assisted the regulation of Bi_2WO_6 oxygen vacancy by iodine doping to introduce oxygen vacancy and induce photocatalytic oxidation of organochlorine pesticides. It was of note that the total organic carbon removal efficiency of sodium pentachlorophenol by iodine-doped Bi_2WO_6 was over 90% within 2 h, which was 10.6 times higher than that of Bi_2WO_6 under visible light. This is mainly caused by the fact that iodine doping weakens the introduction of sufficient oxygen vacancy in the Bi_2WO_6 lattice, thus significantly enhancing the molecular oxygen activity to degrade sodium pentachlorophenol. In addition, phosphorus-doped g-C_3N_4 modified Bi_2WO_6

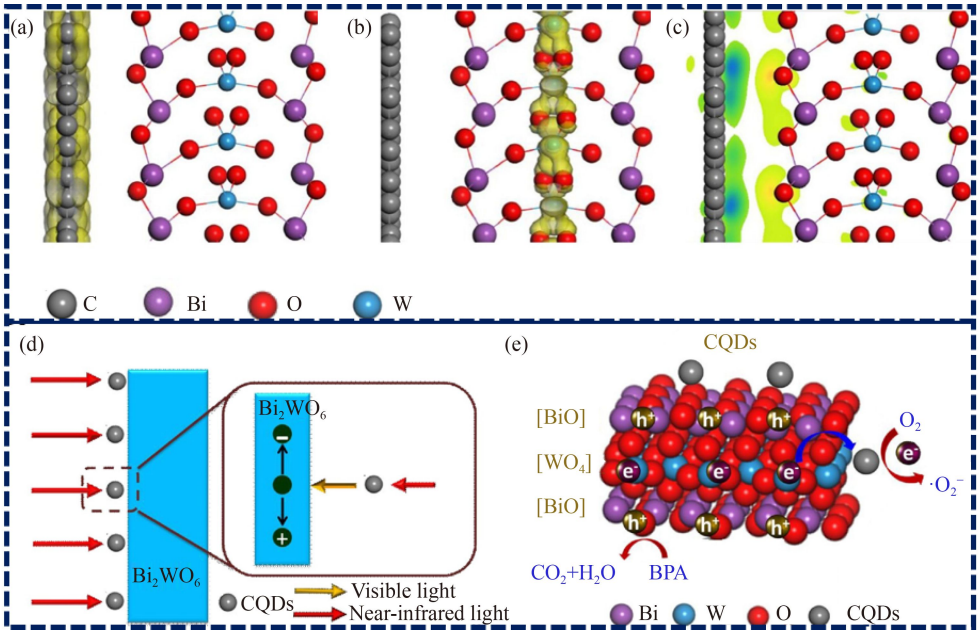

Fig. 8 The distribution of partial charge density of valence band (a) and conduction band (b) of CQDs/m-Bi_2WO_6; (c) Deformation charge density of CQDs/m-Bi_2WO_6; (d) Schematic diagram of PL transformation in CQDs/m-Bi_2WO_6 heterojunction; (e) Photocatalytic mechanism diagram of CQDs/m-Bi_2WO_6 under visible and infrared light irradiation. Reprinted from Ref. (Wang et al., 2018a) with permission from The German Chemical Society.

and AgBr were successfully prepared using a simple *in situ* sedimentation-calcination-hydrothermal method (Xue et al., 2023). The removal efficiency of tetracycline by the composite reached 99.2% within 60 min, primarily because of the facilitation of photogenic carrier separation and low recombination rate based on the formation of mid-gap, Ag bridge, and multiple heterojunctions.

Metal doping improves the photocatalytic performance of composites through adjusting the band gap, and charge density distribution. Ding et al. reported that the photocatalytic removal efficiency of sodium pentachlorophenate was significantly enhanced by bismuth self-doping Bi_2WO_6 using a soft-chemical method (Ding et al., 2014). The results of structure characterization and DFT calculation indicated that bismuth self-doping Bi_2WO_6 improved photogenic carrier separation and transfer to produce more active substances. The introduction of Ti and Zr in Bi_2WO_6 resulted in structural defects and reduced the CB positions, enhancing visible-light responsiveness (Zhang et al., 2011; Arif et al., 2021). In brief, atom doping introduces defects to adjust the band gap and hole and significantly improves the photogenerated electrons and hole migration rate, aiming to increase the photocatalytic activity (Table 2).

4 Application of Bi_2WO_6-based materials in photocatalysis

4.1 Environmental remediation field

4.1.1 Degradation of organic pollutants

With the rapid development of industrial modernization, various organic pollutants, including pharmaceutical and personal care products (PPCPs), persistent organic pollutants (POPs), organic dyes, antibiotics, and pesticides, are constantly entering into the natural environment, posing serious environmental threats on human health and life (Chu et al., 2016; Huang et al., 2016a). As a novel energy-saving and environmental-friendly treatment method, photocatalysis has been considered as a prospective technology for the degradation of organic pollutants.

Zhao et al. (2024b) prepared an n-p type $Bi_2WO_6/AgInS_2$ S-type heterojunction based on hydrothermal method, and this $Bi_2WO_6/AgInS_2$ S-type heterojunction exhibited excellent photocatalytic activity for RhB, norfloxacin (NF), and levofloxacin (LEV) under visible light (Table 3). Similarly, Guo et al. (2020) constructed Bi_2WO_6-BiOCl by hydrothermal reaction, revealing a highly efficient degradation pathway of oxytetracycline. Simultaneously, numerous Bi_2WO_6 based materials can remove multiple organic pollutants (Table 3). The results are mainly attributed to the following two aspects: first, the separation and migration efficiency of photogenerated electrons and hole pairs significantly increased after the modification of Bi_2WO_6; secondly, the active substance was produced rapidly under the condition of light excitation. For example, Liu et al. (2022) constructed the Z-scheme Fe-g-CN/BiWO photo-Fenton system for efficient degradation of TC. In this study, the contribution of free radicals in organic degradation was determined by quenching experiment and EPR analysis. The TC degradation pathway of photo-Fenton system was indicated by LC-MS analysis (Fig. 9(a)). With visible light excitation, photogenerated holes can react with H_2O to produce hydroxyl radicals, and O_2 was reduced by photo-induced electrons to generate superoxide radicals, thereby accelerating the oxidation of TC and

Table 2 Comparison of photocatalytic properties of element doping Bi_2WO_6

Photocatalyst	Doping mode	Photocatalytic activity	Regulatory mechanism	Ref.
S, F-Bi_2WO_6	Nonmetallic	Methyl orange (MO) degradation: 95.4% (120 min) and Cr(VI) reduction: 94.3% (120 min)	Tuning oxygen vacancy	Peng et al. (2023)
CSs-Bi_2WO_6	Nonmetallic	TC degradation: 84.6% (60 min)	High visible light utilization	Jiang et al. (2023)
$I_{0.5}$0-Bi_2WO_6	Nonmetallic	Bisphenol A degradation: 78% (10 min)	Introducing reductive species I^-	Xu et al. (2021)
N-CQDs/Bi_2WO_6	Nonmetallic	TC degradation: 97% (25 min)	Interfacial charge transfer	Zhang et al. (2018b)
$Bi_{2+X}WO_6$	Metal	Sodium pentachlorophenate degradation: 97% (2.15 h)	Interfacial charge transfer	Ding et al. (2014)
Ti-Bi_2WO_6	Transition metal	Cr(VI) reduction: 100% (60 min)	Mediating oxygen vacancy	Arif et al. (2021)
Zr-Bi_2WO_6	Transition metal	RhB degradation: ~100% (20 min)	Mediating oxygen vacancy	Zhang et al. (2011)
Ag-Bi_2WO_6	Transition metal	RhB degradation: 94% (120 min)	Enhanced surface plasmon resonance	Phu et al. (2020)
Sm^{3+}-Bi_2WO_6	Rare earth metal	RhB degradation: ~100% (40 min)	Tuning oxygen vacancy	Liu et al. (2020)
Yb-Bi_2WO_6	Rare earth metal	RhB degradation: 95% (180 min)	Introducing oxygen vacancies	Li et al. (2021b)
Eu-Bi_2WO_6	Rare earth metal	RhB degradation: 78% (60 min)	Influence morphology evolution	Xu et al. (2014)
Ba-Bi_2WO_6	Metal	RhB degradation: 96.3% (50 min)	Construction electron defect	Li et al. (2015)
La-Bi_2WO_6	Rare earth metal	RhB degradation: 90% (99 min)	Interfacial charge transfer	Ning et al. (2022)

Table 3 Degradation of OP by Bi_2WO_6 based materials

Photocatalyst	Synthesis method	Photocatalytic activity	Photocatalysis condition	Ref.
Bi_2WO_6/$AgInS_2$	Hydrothermal	RhB (92.24%, 60 min), NF (81.73%, 90 min), and LEV (87.46%, 90 min)	C_0 = 10 mg/L; t = 90 min; dosage = 0.3 g/L; LS: 300 W Xenon lamp	Zhao et al. (2024b)
I-Bi/Bi_2WO_6	One-step solvothermal	Colorless BPA (30 mg/L, 93%), RhB (10 mg/L, 99.9%), anionic dye CoR (40 mg/L, 91%), sulfamethoxazole (SX, 10 mg/L, 55%), and atrazine (AZ, 10 mg/L, 60%)	t = 60 min; dosage = 0.2 g/L; LS: 300 W Xenon lamp	Hua et al. (2020)
Bi_2WO_6-BiOCl	Hydrothermal and solvothermal	Oxytetracycline (98.5%)	C_0 = 20 mg/L; t = 80 min; dosage = 1 g/L; LS: 500 W Xenon lamp	Guo et al. (2020)
$I_{0.30}$-Bi_2WO_6	Hydrothermal	2-chlorophenol (80%)	C_0 = 10 mg/L; t = 300 min; dosage = 2 mg; LS: 150 W Xenon lamp	Wang et al. (2018c)
Oxygen vacancies enriched Bi_2WO_6	Solvothermal calcination	Decabromodiphenyl ether (BDE209, 98%)	C_0 = 10 mg/L; t = 40 min; dosage = 0.3 g/L; LS: 300 W Xenon lamp	Yang et al. (2022)
CQD/BiOBr/Bi_2WO_6	Hydrothermal	Norfloxacin (k = 0.01717 min^{-1})	C_0 = 15 mg/L; t = 120 min; dosage = 0.1 g/L; LS: 500 W Xenon lamp	Zhang et al. (2022)
Bi_2WO_6/RGO	Hydrothermal	RhB (99.5%), MO (78.5%), phenol (66.5%), SX (70.9%), and sulfanilamide (57.6%)	C_0 = 10 mg/L; t = 8 h; dosage = 0.5 g/L; LS: natural sunlight	Dong et al. (2017)
Cu-Bi_2WO_6-Vo	One step solvothermal	TC (94%)	C_0 = 20 mg/L; t = 30 min; dosage = 0.3 g/L; PMS = 0.3 g/L; LS: 300 W Xenon lamp	Zheng et al. (2023)

interconversion between Fe(II) and Fe(III) to produce more free radicals (Fig. 9(b)). Due to the high electron density, the amine groups, phenolic groups, and double bonds in the TC molecule were susceptible to be attacked by free radicals and holes (Wang et al., 2018b). Currently, pesticides have been widely used in agricultural production, causing excessive organic matter content in agricultural withdrawal water. GokulaKrishnan et al. (2024) anchored Bi_2WO_6 nanoparticles on the membrane by grafting through *in situ* polymerization for treating agricultural regression water.

4.1.2 Cr(VI) photocatalytic removal

As highly toxic substances, Cr(VI), may harm human health and damage the ecological environment. Meanwhile, Cr(VI) is 200 times more toxic than Cr(III) (Zhang et al., 2020b; Mao et al., 2022a). The photoelectrons and holes produced by photoexcitation can effectively lower Cr(VI), which has been regarded as a promising technology to address Cr(VI) pollution.

Arif et al. developed interface engineering of α-MnO_2/Bi_2WO_6 and regulated defect active sites for efficient photocatalytic reduction of Cr(VI) and degradation of TC (Fig. 10(a)) (Arif et al., 2023). The photoinduced charge separation and conversion of α-MnO_2/Bi_2WO_6 were significantly enhanced by surface oxygen vacancies and defective sites Mn(III)/Mn(IV). As displayed in Fig. 10(b), photoexcitation led to the generation of an internal electric field at the heterojunction interface, which could accelerate the migration of photogenerated electrons to the conduction band of α-MnO_2 and holes to the valence band of Bi_2WO_6. In this case, the electrons in the conduction band of α-MnO_2 can directly reduce Cr(VI), while the holes in the valence band of Bi_2WO_6 would probably be capable of producing hydroxyl radicals and oxidize TC, according to the previous study of Bi_2WO_6/CuS (Mao et al., 2021b). Z-scheme PPy/ Bi_2WO_6 composites were synthesized through a polymerization and deposition reaction (Fig. 10(c)) (Song et al., 2022). Due to the internal electric field, the photogenerated electrons on the conduction band of Bi_2WO_6 quickly transferred to the contact interface and reunited with holes on the highest occupied molecular orbital of PPy, promoting the efficient separation and migration of photogenerated carriers on the valence band of Bi_2WO_6 and lowest unoccupied molecular orbital of PPy to produce free radicals. In summary, the photogenerated electrons and free radicals contributed to the reduction of Cr(VI).

Bi_2WO_6 based materials can produce photoelectrons and holes in the photocatalytic reaction, which are characterized by strong reduction and oxidation properties, respectively. Therefore, it can achieve simultaneous oxidation of organic pollutants and detoxification of Cr(VI) in the reaction system. Meanwhile, the photogenic carrier reacts with water and dissolved oxygen to produce free radicals, which can possibly further promote the reduction of Cr(VI). Obviously, the synchronous removal of organic pollutants and Cr(VI) was significantly enhanced in the photocatalytic system. The results are primarily caused by the simultaneous consumption of photogenerated electrons and holes, accelerating the generation and migration of photogenerated carriers (Mao et al., 2021b). As displayed in Fig. 11,Bi_2WO_6 supported on nitrogen-sulfur co-doped BC by solvothermal reaction may promote the efficient transfer of photogenerated electrons, probably accelerating the oxidation of organic matter at the valence band and the reduction of Cr(VI) on the modified BC (Mao et al., 2021a). Similarly, Cai et al. (2023) reported that Bi_2WO_6/C_3N_4/carbon fiber cloth with oxygen vacancy (OV)-rich exhibited an excellent photocatalytic performance for removing antibiotics and Cr(VI).This is mainly resulted from the enhanced active center and accelerated charge carrier disintegration rate

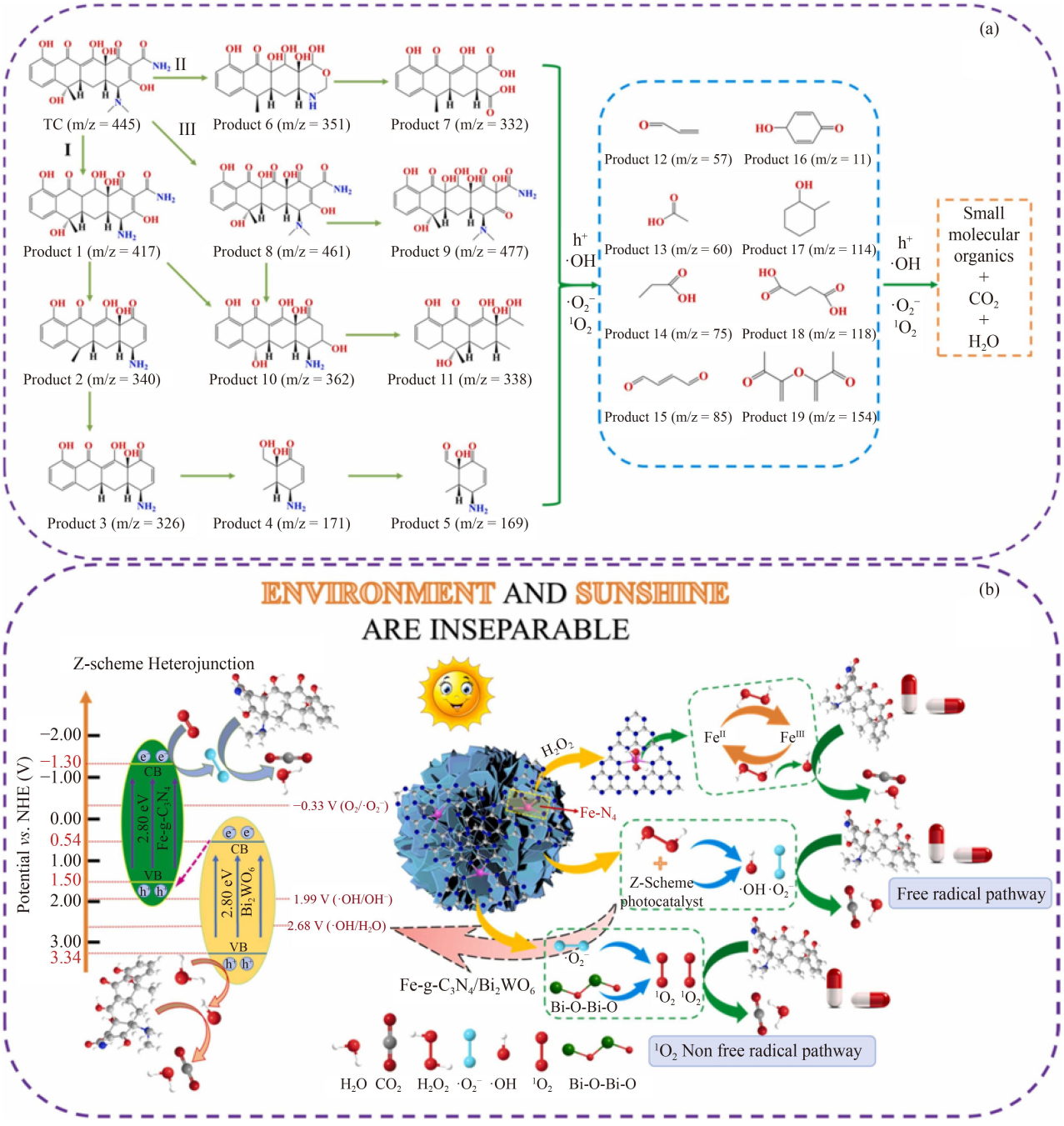

Fig. 9 (a) Degradation path, and (b) photocatalytic removal mechanism of TC by composite materials. Reprinted from Ref. (Liu et al., 2022) with permission from Elsevier.

by constructing a fiber-shaped S-scheme photosystem with OVs.

4.2 Clean energy field

4.2.1 Reduction of CO_2 to high value-added products

Excessive CO_2 emissions from human activities have caused more extreme and frequent weather events including high temperature heat waves, dust storms in some regions, typhoons, and droughts (Hung et al., 2022). Bi_2WO_6-based materials can convert CO_2 into high value-added products under natural light such as CH_4, CH_3OH, CO, HCOOH, and C_2H_5OH (Fig. 12) (Jiang et al., 2017; Li et al., 2020b; Liu et al., 2021b; Collado et al., 2023; Zhao et al., 2024a). During the process of photocatalytic CO_2 reduction, the photogenerated electrons are consumed to reduce CO_2, and the photogenic holes undergo water oxidation reactions. The two C = O (750 kJ/mol) bonds of CO_2 have obviously high bond energies

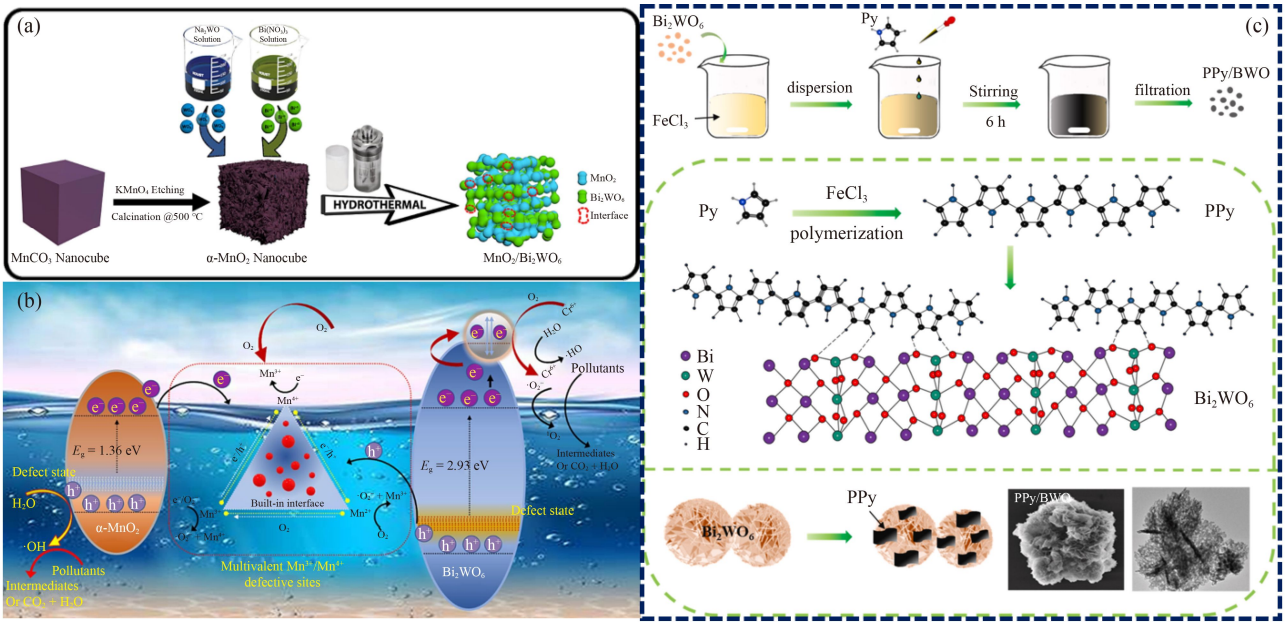

Fig. 10 (a) Preparation flowchart and (b) photocatalytic charge transfer mechanism at internal interface α-MnO_2/Bi_2WO_6 heterostructure; Schematic diagram of (c) photocatalyst preparation of PPy/Bi_2WO_6. Reprinted from Ref. (Song et al., 2022; Arif et al., 2023) with permission from Elsevier.

when compared with the C–H (430 kJ/mol) and C–C (336 kJ/mol) bond (Wu et al., 2017; Shang et al., 2023). Therefore, the photocatalytic CO_2 reduction process needs to provide sufficient energy for ensuring that the reaction goes smoothly. As a result, the modification of Bi_2WO_6 has been widely used with two strategies being included. The photocatalytic performance of Bi_2WO_6 was improved by boosting photoabsorption, local surface plasmon resonance, and metallic photocatalysts, improving carrier separation capability, controlling the microscopic morphology, and so on (Zhao et al., 2023). Lu et al. (2021) constructed surface plasmon resonance on Bi_2WO_6 by electron doping to promote CO_2 selective reduction. It is of note that during the preparation and modification of Bi_2WO_6, the conduction band position should be lower than the reduction potential of CO_2, while the valence band position should be higher than the oxidation potential of H_2O (Zhang et al., 2012). In addition, the contact efficiency between Bi_2WO_6 and CO_2 was enhanced by improving the specific surface area and surface structure. Liu et al. (2021c) constructed a hydrophobic Bi_2WO_6 nanosheets by hexadecyl trimethyl ammonium bromide modification, significantly improving the adsorption and mass-transfer of CO_2 on the surface of Bi_2WO_6. Wang et al. (2023b) designed inner-to-outer tandem homojunctions through gradient cationic

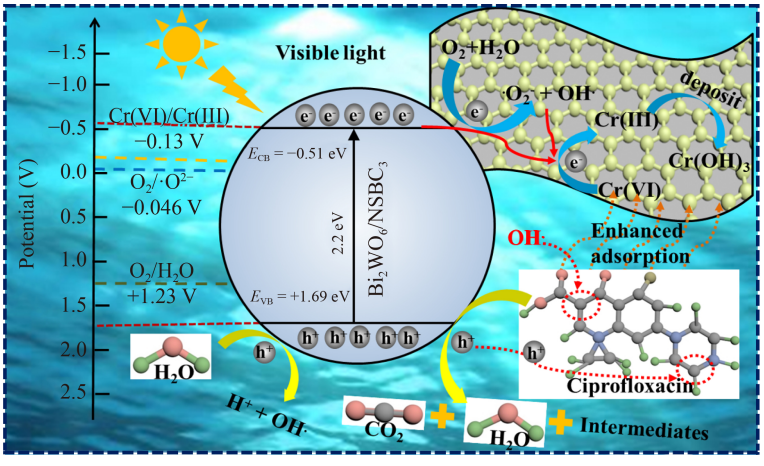

Fig. 11 Possible mechanism for photocatalytic removal of antibiotics and Cr(VI) on Bi_2WO_6/NSBC. Reprinted from Ref. (Mao et al., 2021a) with permission from Elsevier.

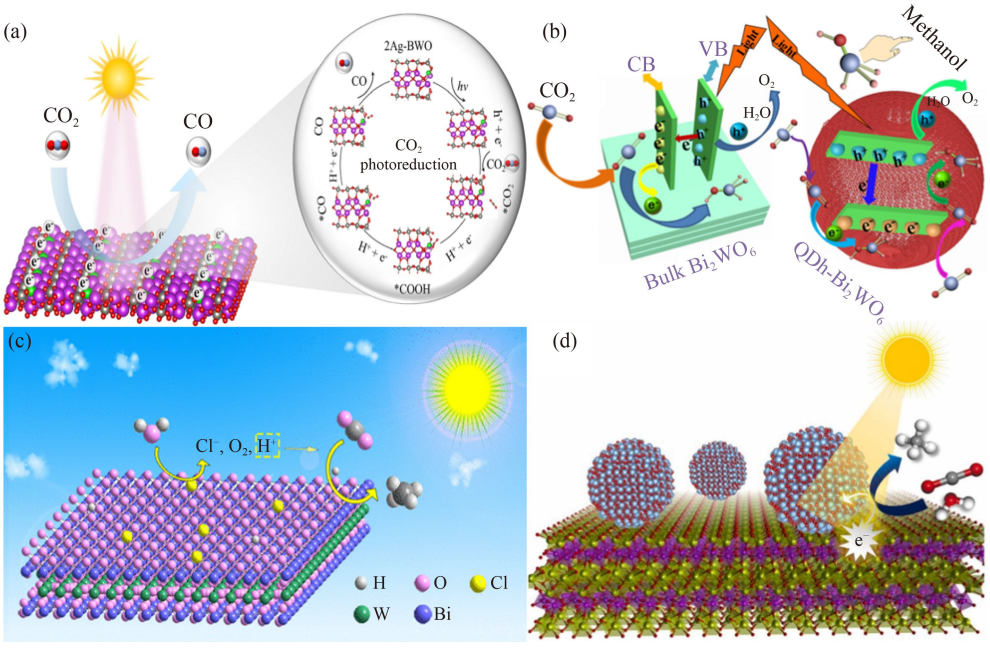

Fig. 12 Schematic diagram of photocatalytic CO_2 reduction mechanism: (a) ultrathin 2Ag-BWO nanosheets, (b) QDh-Bi_2WO_6, (c) chloride-modified Bi_2WO_6, and (d) Bi_2WO_6/TiO_2. Reprinted from Ref. (Jiang et al., 2017; Li et al., 2020b; Collado et al., 2023; Zhao et al., 2024a) with permission from Elsevier, The Royal Society of Chemistry, and Catalysis Society of Chinese Chemical Society, respectively.

vacancies, which may significantly enhance W-vacant Bi_2WO_6 photoreduction of CO_2 through strong local internal electric field and reformed basic sites.

4.2.2 Solar hydrogen production

Owing to its thin two-dimensional structure and electron-dominated lattice, Bi_2WO_6 has the potential to efficiently produce hydrogen gas. The redox potential and suitable band gap of Bi_2WO_6 are the vital factors for hydrogen evolution (Fig. 13) (Wu et al., 2020; Yan et al., 2022). Xing et al. (2019) synthesized ultrathin 2D-2D heterojunctions Bi_2WO_6-Bi_2O_2S through a simple two-step hydrothermal method. A five-alternating-layer sandwich structure was formed by *in situ* growing of Bi_2O_2S, which could not only promote the interfacial charge transfer but also significantly improve the photocatalytic water decomposition efficiency. Some researchers assembled Bi_2WO_6 with other materials due to its excellent optical properties, improving the photocatalytic hydrogen evolution performance of composite materials. Hu et al. (2019) succeeded in introducing black phosphorus into Bi_2WO_6 (BP-Bi_2WO_6) to break down water molecules in the air. The photocatalytic hydrogen evolution rate of BP-Bi_2WO_6 was significantly improved, and was 9.15 times higher than that of pure Bi_2WO_6. Likewise, Murugan et al. (2021) designed S doped-g-C_3N_4/Bi_2WO_6 heterojunction by ultrasonic method. S doped-g-C_3N_4 was combined to form heterojunction structure, thereby accelerating the separation of photogenerated electron-hole pairs, and boosting the water oxidation kinetics on the surface of S doped-g-C_3N_4/Bi_2WO_6.

4.2.3 Ammonia synthesis by nitrogen photocatalytic reduction

Ammonia is a particularly important chemical product in the rapid development of the current industrialization, and has been widely used in agriculture, industry, and military fields. The Haber–Bosch method has been applied in industrial production to synthesize ammonia, which not only consumes 2% of global energy, but also accounts for 1% of the world's annual CO_2 emissions. However, photocatalytic nitrogen fixation refers to the use of abundant clean solar energy input to produce ammonia, obviously meeting the clean production. Dhanaraman et al. (2024) reasonably inserted a Bi_2WO_6 into g-C_3N_4 to enhance photocatalytic antibiotic removal and nitrogen reduction reactions. Verma et al. (2023) successfully optimized the Bi_2WO_6–BiOCl heterojunctions by varying the molar ratio of chlorine: tungsten precursor. The ammonia yield of the Bi_2WO_6–BiOCl was 345.1 umol/(L·h), which was 2.6 and ~2 times higher than that of the original Bi_2WO_6 and BiOCl, respectively. To improve the efficiency of ammonia synthesis, numerous studies have chosen to combine photocatalysis with electrocatalysis to achieve efficient nitrogen reduction of ammonia production. Yang et al. (2021) doped cerium into Bi_2WO_6 by a defection-induced manner for

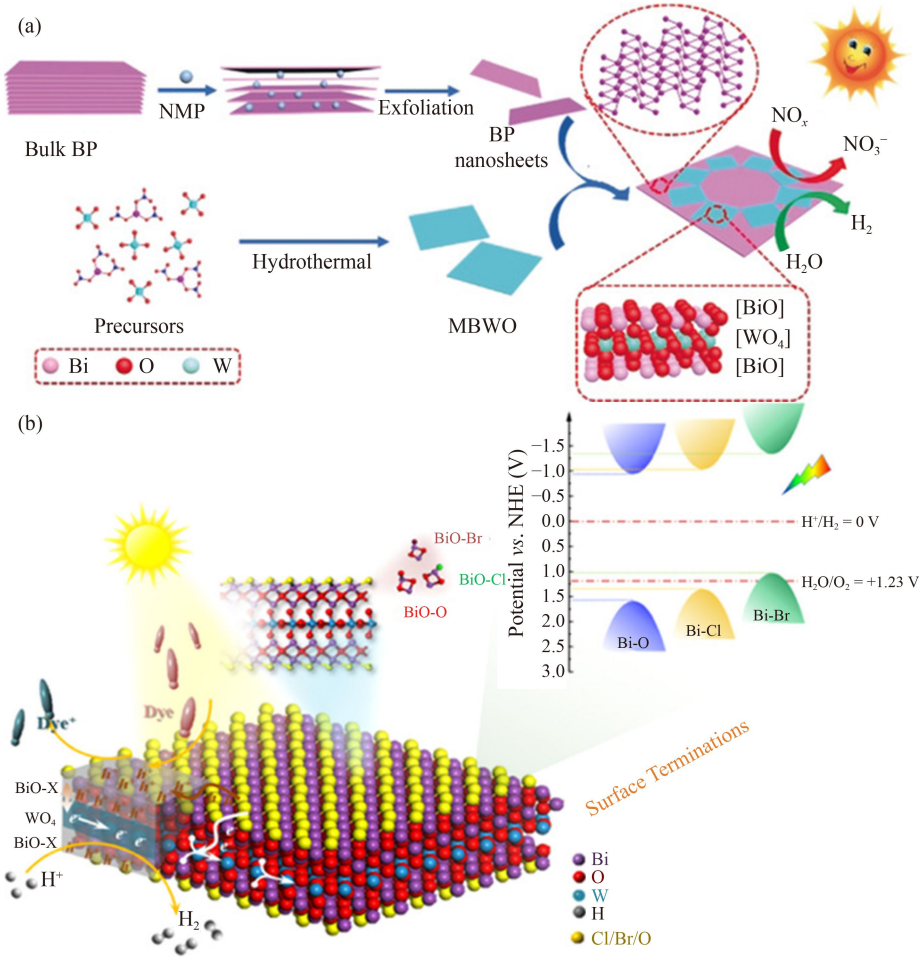

Fig. 13 Schematic diagram of photocatalytic hydrogen production: (a) MBWO and (b) BP-Bi_2WO_6. Reprinted from Ref. (Hu et al., 2019; Wu et al., 2020) with permission from The American Chemical Society and The German Chemical Society.

electrochemical nitrogen reduction of ammonia production.

4.3 Medical science field

The Bi_2WO_6 nanoparticles had an extremely surface activity for photocatalytic oxidation reactions, producing active substances ($\cdot O_2^-$, $\cdot OH$, and $^1O_2$) under light excitation in the range of ultraviolet to near-infrared (Zhou et al., 2015). Thus, many researchers have applied Bi_2WO_6 in photodynamic therapy of tumor (Fig. 14). Wang et al. indicated that Bi_2WO_6 could generate an active substance in the absence of oxygen consumption, opening up novel ideas for oxygen-free photodynamic treatment of tumors (Zhang et al., 2018a). Meanwhile, the Bi_2WO_6 nanoparticles were hired considering their capacity to induce both oxygen-independent type I photodynamic therapy and photothermal therapy (Zhang et al., 2018a). Zhang et al. (2020a) constructed a hybrid by loading oxygen-independent photodynamic Bi_2WO_6 onto a platelet membrane (PM-Bi_2WO_6 NPs). After the hybrid entered the tumor cells, photoexcited Bi_2WO_6 produces enormous quantities of active substances through photodynamic and photothermal processes, which could not only destroy platelet membranes in hypoxic conditions but also overcome the immunosuppression induced by myeloid-derived suppressor cells. Ding et al. synthesized oxygen-deficient and iron-doped Bi_2WO_6 nanosheets (BWO-Fe NSs) with Fenton reaction for enhanced sonodynamic therapy against breast cancer (Ding et al., 2023).

5 Summary and future perspective

5.1 Summary

In this study, the photocatalytic properties of Bi_2WO_6-based materials were improved through adjusting the surface morphology, band gap and electron migration. In addition, the advanced applications in the fields of environmental pollution remediation, life medicine and clean energy were reviewed. The continuous breakthrough of controllable preparation and modification nano-

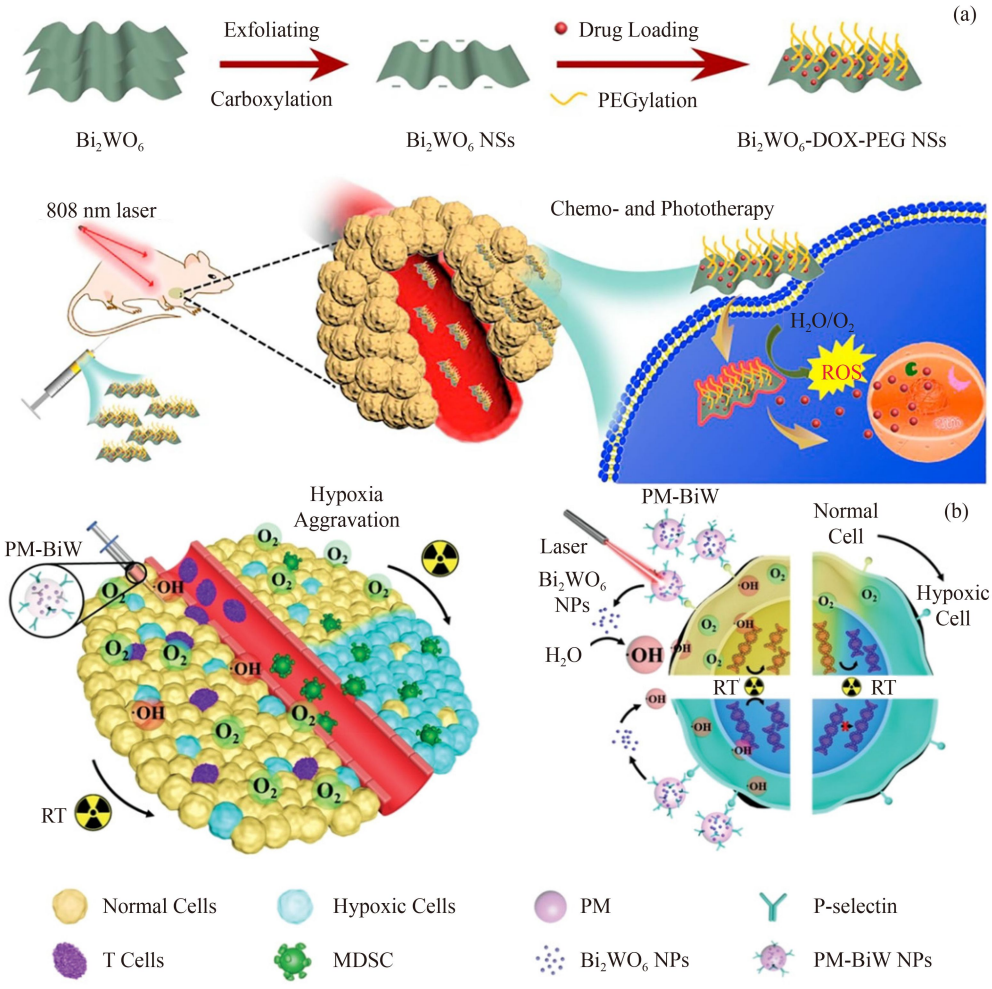

Fig. 14 Schematic diagram of anti-tumor mechanism: (a) Bi_2WO_6-DOX-PEG NSs and (b) PM-BiW NPs. Reprinted from Ref. (Feng et al., 2018; Zhang et al., 2020a) with permission from Elsevier, and Wiley, respectively.

structured Bi_2WO_6-based materials, including atomic doping, carbon loading and heterostructural construction, has brought specific surface area, photoelectron-hole migration ability, visible light response range and band gap width, etc., thus exerting a significant role in improving photocatalytic performance.

Since the photocatalytic properties of Bi_2WO_6-based materials are primarily influenced by photoelectron-hole migration and visible light absorption range, the effective improvement on their surface structure and bonding bonds are vital factors to determine the photocatalytic performance. For example, the successful loading of Bi_2WO_6 on the modified carbon-based material may achieve effective photogenic electron transfer and adsorption-removal of pollutants in the composite material, exhibiting strong chemical and structural advantages. The photocatalytic process produces strong oxidizing holes, which can achieve efficient removal of organic matter. In addition, the photogenerated electrons formed may achieve CO_2 reduction and water decomposition, effectively realizing the conversion of solar energy to chemical energy. During the photocatalytic process, the Bi_2WO_6-based material will release numerous active substances, which can also be used as a medium for tumor photodynamic therapy.

5.2 Future perspective

However, there are still some shortcomings in the research of Bi_2WO_6-based materials. The existing limitations should be further considered in the future studies.

1) Machine learning is expected to be incorporated into the construction process of Bi_2WO_6-based materials to assist in modifying photocatalysts in a data-driven manner, which can realize full exposure of active sites in the structure of Bi_2WO_6 perovskite.

2) Although atomic modulation can change the photocatalytic performance of Bi_2WO_6, it is difficult to accurately regulate the atomic sites. Therefore, it is essential to employ reasonable design and advanced characterization techniques to further show the

mechanism of atomic sites in the photocatalytic reaction.

3) The modification of Bi_2WO_6-based materials mainly improves the electron and hole migration rate of composites. However, the mechanism of photogenerated carrier migration at the interface remains controversial. Therefore, the *in situ* characterization method needs to be developed to analyze the interfacial charge dynamics and identify the photogenerated electron-hole migration process at the interfacial of Bi_2WO_6-based materials.

4) The photocatalytic process mainly depends on the oxidation or reduction of photogenerated carrier, while the contact between Bi_2WO_6-based materials and water is limited. Thus, the active substances decrease one by one with the distance during the reaction. Moreover, it is essential to introduce an intermediate medium that can act as an energy medium to satisfy the homogeneous redox reaction in the system.

5) To improve the treatment effect, Bi_2WO_6-based materials may be effectively combined with electrocatalysis, ultrasonic and thermal catalysis to further enhance the release of active substances and photocatalytic activity.

Acknowledgements This work was supported by the National Natural Science Foundation of China (No. 52300209); the Guangdong Higher Education Institutions Innovative Research Team of Urban Water Cycle and Ecological Safety (China) (No. 2023KCXTD053); and the Shenzhen Science and Technology Innovation Commission (China) (Nos. WDZC20200821090937001 and KCXST20221021111401004); and the Scientific Research Start-up Funds from Tsinghua Shenzhen International Graduate School (China) (No. QD2023020C).

Conflict of Interests The authors declare that the research was conducted in the absence of any commercial or financial relationships that could be construed as a potential conflict of interest.

References

Arif M, Mahsud A, Ali A, Liao S, Xia J, Xiao H, Azam M, Muhmood T, Lu Z, Chen Y (2023). Unraveling the synergy of interface engineering α-MnO_2/Bi_2WO_6 heterostructures and defective active sites for superdurable photocatalysis: mechanistic insights into charge separation/transfer. Chemical Engineering Journal, 475: 146458

Arif M, Zhang M, Mao Y, Bu Q, Ali A, Qin Z, Muhmood T, Shahnoor, Liu X, Zhou B, Chen S (2021). Oxygen vacancy mediated single unit cell Bi_2WO_6 by Ti doping for ameliorated photocatalytic performance. Journal of Colloid and Interface Science, 581: 276–291

Bai Y, Mao W, Wu Y, Gao Y, Wang T, Liu S (2021). Synthesis of novel ternary heterojunctions via Bi_2WO_6 coupling with CuS and g-C_3N_4 for the highly efficient visible-light photodegradation of ciprofloxacin in wastewater. Colloids and Surfaces. A, Physicochemical and Engineering Aspects, 610: 125481

Bai Y, Wang T, Zhao X, Mao W, Liu S (2020). Synthesis of novel ternary Bi_2WO_6/CeO_2/g-C_3N_4 composites with enhanced visible light photocatalytic activity for removal of organic and Cr(VI) from wastewater. Journal of Materials Science Materials in Electronics, 31(20): 17524–17534

Cai M, Liu Y, Dong K, Chen X, Li S (2023). Floatable S-scheme Bi_2WO_6/C_3N_4/carbon fiber cloth composite photocatalyst for efficient water decontamination. Chinese Journal of Catalysis, 52: 239–251

Cao H, Liu F, Tai Y, Wang W, Li X, Li P, Zhao H, Xia Y, Wang S (2023). Promoting photocatalytic performance of TiO_2 nanomaterials by structural and electronic modulation. Chemical Engineering Journal, 466: 143219

Cao X, Yue L, Lian F, Wang C, Cheng B, Lv J, Wang Z, Xing B (2021). CuO nanoparticles doping recovered the photocatalytic antialgal activity of graphitic carbon nitride. Journal of Hazardous Materials, 403: 123621

Chen L, Wang C, Liu G, Su G, Ye K, He W, Li H, Wei H, Dang L (2023). Anchoring black phosphorous quantum dots on Bi_2WO_6 porous hollow spheres: a novel 0D/3D S-scheme photocatalyst for efficient degradation of amoxicillin under visible light. Journal of Hazardous Materials, 443: 130326

Chen T, Liu L, Hu C, Huang H (2021). Recent advances on Bi_2WO_6-based photocatalysts for environmental and energy applications. Chinese Journal of Catalysis, 42(9): 1413–1438

Cheng Y, Chen J, Wang P, Liu W, Che H, Gao X, Liu B, Ao Y (2022). Interfacial engineering boosting the piezocatalytic performance of Z-scheme heterojunction for carbamazepine degradation: Mechanism, degradation pathway and DFT calculation. Applied Catalysis B: Environmental, 317: 121793

Chu X, Shan G, Chang C, Fu Y, Yue L, Zhu L (2016). Effective degradation of tetracycline by mesoporous Bi_2WO_6 under visible light irradiation. Frontiers of Environmental Science & Engineering, 10(2): 211–218

Collado L, Gomez-Mendoza M, García-Tecedor M, Oropeza F E, Reynal A, Durrant J R, Serrano D P, de la Peña O'Shea V A (2023). Towards the improvement of methane production in CO_2 photoreduction using Bi_2WO_6/TiO_2 heterostructures. Applied Catalysis B: Environmental, 324: 122206

Cui Y, Wang T, Liu J, Hu L, Nie Q, Tan Z, Yu H (2021). Enhanced solar photocatalytic degradation of nitric oxide using graphene quantum dots/bismuth tungstate composite catalysts. Chemical Engineering Journal, 420: 129595

Dhanaraman E, Verma A, Chen P H, Chen N D, Siddiqui Y, Fu Y P (2024). Bi_2WO_6 incorporation of g-C_3N_4 to enhance the photocatalytic N_2 reduction reaction and antibiotic pollutants removal. Solar RRL, 8: 2300981

Ding X, Zhao K, Zhang L (2014). Enhanced photocatalytic removal of

sodium pentachlorophenate with self-doped Bi_2WO_6 under visible light by generating more superoxide ions. Environmental Science & Technology, 48(10): 5823–5831

Ding Y, Zhao Y, Yao S, Wang S, Wan X, Hu Q, Li L (2023). Enhanced sonodynamic cancer therapy through iron–doping and oxygen–vacancy engineering of piezoelectric bismuth tungstate nanosheets. Small, 19(24): 2300327

Dong S, Ding X, Guo T, Yue X, Han X, Sun J (2017). Self-assembled hollow sphere shaped Bi_2WO_6/RGO composites for efficient sunlight-driven photocatalytic degradation of organic pollutants. Chemical Engineering Journal, 316: 778–789

Fehr A M K, Agrawal A, Mandani F, Conrad C L, Jiang Q, Park S Y, Alley O, Li B, Sidhik S, Metcalf I, et al. (2023). Integrated halide perovskite photoelectrochemical cells with solar-driven water-splitting efficiency of 20.8%. Nature Communications, 14(1): 3797

Feng L, Yang D, Gai S, He F, Yang G, Yang P, Lin J (2018). Single bismuth tungstate nanosheets for simultaneous chemo-, photothermal, and photodynamic therapies mediated by near-infrared light. Chemical Engineering Journal, 351: 1147–1158

Feng X, Zheng R, Gao C, Wei W, Peng J, Wang R, Yang S, Zou W, Wu X, Ji Y, et al. (2022). Unlocking bimetallic active sites via a desalination strategy for photocatalytic reduction of atmospheric carbon dioxide. Nature Communications, 13(1): 2146

GokulaKrishnan S A, Arthanareeswaran G, Devi D R (2024). Bi_2WO_6 nanoparticles anchored on membrane by grafting via *in-situ* polymerization for the treatment of antibiotic and pesticides wastewater. Chemosphere, 351: 141214

Guo M, Zhou Z, Yan S, Zhou P, Miao F, Liang S, Wang J, Cui X (2020). Bi_2WO_6–BiOCl heterostructure with enhanced photocatalytic activity for efficient degradation of oxytetracycline. Scientific Reports, 10(1): 18401

Guo X, Zhang F, Zhang Y, Hu J (2023). Review on the advancement of SnS_2 in photocatalysis. Journal of Materials Chemistry. A, Materials for Energy and Sustainability, 11(14): 7331–7343

Haider S, Nawaz R, Anjum M, Haneef T, Oad V K, Uddinkhan S, Khan R, Aqif M (2023). Property-performance relationship of core-shell structured black TiO_2 photocatalyst for environmental remediation. Frontiers of Environmental Science & Engineering, 17(9): 111

He Y, Lv H, Daili Y, Yang Q, Junior L B, Liu D, Liu H, Ma Z (2020). Construction of a new cascade photogenerated charge transfer system for the efficient removal of bio-toxic levofloxacin and Rhodamine B from aqueous solution: mechanism, degradation pathways and intermediates study. Environmental Research, 187: 109647

He Z, Siddique M S, Yang H, Xia Y, Su J, Tang B, Wang L, Kang L, Huang Z (2022). Novel Z-scheme In_2S_3/Bi_2WO_6 core-shell heterojunctions with synergistic enhanced photocatalytic degradation of tetracycline hydrochloride. Journal of Cleaner Production, 339: 130634

Hu J, Chen D, Mo Z, Li N, Xu Q, Li H, He J, Xu H, Lu J (2019). Z-scheme 2D/2D eterojunction of black phosphorus/monolayer Bi_2WO_6 nanosheets with enhanced photocatalytic activities. Angewandte Chemie International Edition, 58(7): 2073–2077

Hua C, Wang J, Dong X, Wang Y, Zheng N, Xue M, Zhang X (2020). *In situ* plasmonic Bi grown on I-doped Bi_2WO_6 for enhanced visible-light-driven photocatalysis to mineralize diverse refractory organic pollutants. Separation and Purification Technology, 250: 117119

Huang Y, Fan W, Long B, Li H, Zhao F, Liu Z, Tong Y, Ji H (2016a). Visible light $Bi_2S_3/Bi_2O_3/Bi_2O_2CO_3$ photocatalyst for effective degradation of organic pollutions. Applied Catalysis B: Environmental, 185: 68–76

Huang Y, Guo Z, Liu H, Zhang S, Wang P, Lu J, Tong Y (2019). Heterojunction architecture of N-doped WO_3 nanobundles with Ce_2S_3 nanodots hybridized on a carbon textile enables a highly efficient flexible photocatalyst. Advanced Functional Materials, 29(45): 1903490

Huang Y, Long B, Tang M, Rui Z, Balogun M S, Tong Y, Ji H (2016b). Bifunctional catalytic material: an ultrastable and high-performance surface defect CeO_2 nanosheets for formaldehyde thermal oxidation and photocatalytic oxidation. Applied Catalysis B: Environmental, 181: 779–787

Hung S F, Xu A, Wang X, Li F, Hsu S H, Li Y, Wicks J, Cervantes E G, Rasouli A S, Li Y C, et al. (2022). A metal-supported single-atom catalytic site enables carbon dioxide hydrogenation. Nature Communications, 13(1): 819

Jiang X, Chen S, Zhang X, Qu L, Qi H, Wang B, Xu B, Huang Z (2023). Carbon-doped flower-like Bi_2WO_6 decorated carbon nanosphere nanocomposites with enhanced visible light photocatalytic degradation of tetracycline. Advanced Composites and Hybrid Materials, 6(1): 47

Jiang Z, Liang X, Zheng H, Liu Y, Wang Z, Wang P, Zhang X, Qin X, Dai Y, Whangbo M H, et al. (2017). Photocatalytic reduction of CO_2 to methanol by three-dimensional hollow structures of Bi_2WO_6 quantum dots. Applied Catalysis B: Environmental, 219: 209–215

Kang F, Jiang X, Wang Y, Ren J, Xu B B, Gao G, Huang Z, Guo Z (2023). Electron-rich biochar enhanced Z-scheme heterojunctioned bismuth tungstate/bismuth oxyiodide removing tetracycline. Inorganic Chemistry Frontiers, 10(20): 6045–6057

Keerthana S P, Rani B J, Ravi G, Yuvakkumar R, Hong S I, Velauthapillai D, Saravanakumar B, Thambidurai M, Dang C (2020). Ni doped Bi_2WO_6 for electrochemical OER activity. International Journal of Hydrogen Energy, 45(38): 18859–18866

Kochanek J, Soo R M, Martinez C, Dakuidreketi A, Mudge A M (2022). Biochar for intensification of plant-related industries to meet productivity, sustainability and economic goals: a review. Resources, Conservation and Recycling, 179: 106109

Li C, Zhao Z, Fu S, Wang X, Ma Y, Dong S (2021a). Polyvinylpyrrolidone in the one-step synthesis of carbon quantum dots anchored hollow microsphere Bi_2WO_6 enhances the simultaneous photocatalytic removal of tetracycline and Cr(VI). Separation and Purification Technology, 270: 118844

Li J, Liang Z, Qin Y, Guo L, Lei N, Song Q (2018). Defective Bi_2WO_6-supported Cu nanoparticles as efficient and stable photoelectrocatalytic for water splitting in near-neutral media. Energy Technology, 6(11): 2247–2255

Li K, Lu X, Zhang Y, Liu K, Huang Y, Liu H (2020a). Bi_3TaO_7/Ti_3C_2 heterojunctions for enhanced photocatalytic removal of water-borne contaminants. Environmental Research, 185: 109409

Li W T, Huang W Z, Zhou H, Yin H Y, Zheng Y F, Song X C (2015). Synthesis and photoactivity enhancement of Ba doped Bi_2WO_6

photocatalyst. Materials Research Bulletin, 64: 432–437

Li X, Li W, Gu S, Liu X, Li H, Ren C, Ma X, Zhou H (2021b). Efficient ytterbium-doped Bi_2WO_6 photocatalysts: synthesis, the formation of oxygen vacancies and boosted superoxide yield for enhanced visible-light photocatalytic activity. Journal of Alloys and Compounds, 851: 156935

Li Y Y, Fan J S, Tan R Q, Yao H C, Peng Y, Liu Q C, Li Z J (2020b). Selective photocatalytic reduction of CO_2 to CH_4 modulated by chloride modification on Bi_2WO_6 nanosheets. ACS Applied Materials & Interfaces, 12(49): 54507–54516

Li Y, Gu M, Zhang X, Fan J, Lv K, Carabineiro S A C, Dong F (2020c). 2D g-C_3N_4 for advancement of photo-generated carrier dynamics: Status and challenges. Materials Today, 41: 270–303

Lin K T, Cheng W H, Cheng H L, Lin H H, Chou W Y, Hsu B Y, Mao C A, Hou Y C, Ruan J (2023). Photocatalytic hydrogen evolution enabled by oriented phase interactions between monolayers of P3HT-wrapped MoS_2 and ferroelectric lamellar crystals. Advanced Functional Materials, 34: 2307262

Liu C, Dai H, Tan C, Pan Q, Hu F, Peng X (2022). Photo-Fenton degradation of tetracycline over Z-scheme Fe-g-C_3N_4/Bi_2WO_6 heterojunctions: mechanism insight, degradation pathways and DFT calculation. Applied Catalysis B: Environmental, 310: 121326

Liu L, Liu J, Sun K, Wan J, Fu F, Fan J (2021a). Novel phosphorus-doped Bi_2WO_6 monolayer with oxygen vacancies for superior photocatalytic water detoxication and nitrogen fixation performance. Chemical Engineering Journal, 411: 128629

Liu S, Wang C, Wu J, Tian B, Sun Y, Lv Y, Mu Z, Sun Y, Li X, Wang F, et al. (2021b). Efficient CO_2 electroreduction with a monolayer Bi_2WO_6 through a metallic intermediate surface state. ACS Catalysis, 11(20): 12476–12484

Liu X, Zhao Y, Ni Y, Shi F, Guo X, Li C (2023). Hydroxylated organic semiconductors for efficient photovoltaics and photocatalytic hydrogen evolution. Energy & Environmental Science, 16(9): 4065–4072

Liu Y, Shen D, Zhang Q, Lin Y, Peng F (2021c). Enhanced photocatalytic CO_2 reduction in H_2O vapor by atomically thin Bi_2WO_6 nanosheets with hydrophobic and nonpolar surface. Applied Catalysis B: Environmental, 283: 119630

Liu Y, Tang H, Lv H, Li Z, Ding Z, Li S (2014). Self-assembled three-dimensional hierarchical Bi_2WO_6 microspheres by sol–gel–hydro-thermal route. Ceramics International, 40(4): 6203–6209

Liu Z, Liu X, Wei L, Yu C, Yi J, Ji H (2020). Regulate the crystal and optoelectronic properties of Bi_2WO_6 nanosheet crystals by Sm^{3+} doping for superior visible-light-driven photocatalytic performance. Applied Surface Science, 508: 145309

Lu C, Li X, Wu Q, Li J, Wen L, Dai Y, Huang B, Li B, Lou Z (2021). Constructing surface plasmon resonance on Bi_2WO_6 to boost high-selective CO_2 reduction for methane. ACS Nano, 15(2): 3529–3539

Ma D, Zhang Z, Zou Y, Chen J, Shi J W (2024). The progress of g-C_3N_4 in photocatalytic H_2 evolution: from fabrication to modification. Coordination Chemistry Reviews, 500: 215489

Ma Y, Liu Q, Wang Q, Qu D, Shi J (2016). Insight into the origin of photoreactivity of various well-defined Bi_2WO_6 crystals: exposed heterojunction-like surface and oxygen defects. RSC Advances, 6(23): 18916–18923

Mao W, Wang T, Wang H, Zou S, Liu S (2018). Novel Bi_2WO_6 loaded g-C_3N_4 composites with enhanced photocatalytic degradation of dye and pharmaceutical wastewater under visible light irradiation. Journal of Materials Science Materials in Electronics, 29(17): 15174–15182

Mao W, Zhang L, Liu Y, Wang T, Bai Y, Guan Y (2021a). Facile assembled N, S-codoped corn straw biochar loaded Bi_2WO_6 with the enhanced electron-rich feature for the efficient photocatalytic removal of ciprofloxacin and Cr(VI). Chemosphere, 263: 127988

Mao W, Zhang L, Wang T, Bai Y, Guan Y (2021b). Fabrication of highly efficient Bi_2WO_6/CuS composite for visible-light photocatalytic removal of organic pollutants and Cr(VI) from wastewater. Frontiers of Environmental Science & Engineering, 15(4): 52

Mao W, Zhang L, Zhang Y, Guan Y (2022a). Simultaneous removal of arsenite and cadmium by a manganese-crosslinking sodium alginate modified biochar and zerovalent iron composite from aqueous solutions. Environmental Science. Nano, 9(1): 214–228

Mao W, Zhang L, Zhang Y, Wang Y, Wen N, Guan Y (2022b). Adsorption and photocatalysis removal of arsenite, arsenate, and hexavalent chromium in water by the carbonized composite of manganese-crosslinked sodium alginate. Chemosphere, 292: 133391

Mao W, Zhang Y, Luo J, Chen L, Guan Y (2022c). Novel co-polymerization of polypyrrole/polyaniline on ferrate modified biochar composites for the efficient adsorption of hexavalent chromium in water. Chemosphere, 303: 135254

Meng X, Li Z, Zeng H, Chen J, Zhang Z (2017). MoS_2 quantum dots-interspersed Bi_2WO_6 heterostructures for visible light-induced detoxification and disinfection. Applied Catalysis B: Environmental, 210: 160–172

Monisha R S, Mani R L, Sivaprakash B, Rajamohan N, Vo D V N (2022). Green remediation of pharmaceutical wastes using biochar: a review. Environmental Chemistry Letters, 20(1): 681–704

Monticelli S, Talbot A, Gotico P, Caillé F, Loreau O, Del Vecchio A, Malandain A, Sallustrau A, Leibl W, Aukauloo A, et al. (2023). Unlocking full and fast conversion in photocatalytic carbon dioxide reduction for applications in radio-carbonylation. Nature Communications, 14(1): 4451

Murugan C, Ranjithkumar K, Pandikumar A (2021). Interfacial charge dynamics in type-II heterostructured sulfur doped-graphitic carbon nitride/bismuth tungstate as competent photoelectrocatalytic water splitting photoanode. Journal of Colloid and Interface Science, 602: 437–451

Ng B J, Putri L K, Kong X Y, Teh Y W, Pasbakhsh P, Chai S P (2020). Z-scheme photocatalytic systems for solar water splitting. Advanced Science, 7(7): 1903171

Ning J, Zhang J, Dai R, Wu Q, Zhang L, Zhang W, Yan J, Zhang F (2022). Experiment and DFT study on the photocatalytic properties of La-doped Bi_2WO_6 nanoplate-like materials. Applied Surface Science, 579: 152219

Orimolade B O, Idris A O, Feleni U, Mamba B (2021). Recent advances in degradation of pharmaceuticals using Bi_2WO_6 mediated photocatalysis: a comprehensive review. Environmental Pollution, 289: 117891

Osman A I, Fawzy S, Farghali M, El-Azazy M, Elgarahy A M, Fahim R A, Maksoud M I A A, Ajlan A A, Yousry M, Saleem Y, et al.

(2022). Biochar for agronomy, animal farming, anaerobic digestion, composting, water treatment, soil remediation, construction, energy storage, and carbon sequestration: a review. Environmental Chemistry Letters, 20(4): 2385–2485

Peng D Y, Zeng H Y, Xiong J, Liu F Y, Wang L H, Xu S, Yang Z L, Liu S G (2023). Tuning oxygen vacancy in Bi_2WO_6 by heteroatom doping for enhanced photooxidation-reduction properties. Journal of Colloid and Interface Science, 629: 133–146

Phu N D, Hoang L H, Chen X B, Kong M H, Wen H C, Chou W C (2015). Study of photocatalytic activities of Bi_2WO_6 nanoparticles synthesized by fast microwave-assisted method. Journal of Alloys and Compounds, 647: 123–128

Phu N D, Hoang L H, Van Hai P, Huy T Q, Chen X B, Chou W C (2020). Photocatalytic activity enhancement of Bi_2WO_6 nanoparticles by Ag doping and Ag nanoparticles modification. Journal of Alloys and Compounds, 824: 153914

Qian X, Yue D, Tian Z, Reng M, Zhu Y, Kan M, Zhang T, Zhao Y (2016). Carbon quantum dots decorated Bi_2WO_6 nanocomposite with enhanced photocatalytic oxidation activity for VOCs. Applied Catalysis B: Environmental, 193: 16–21

Rajaji U, Govindasamy M, Chen S M, Chen T W, Liu X, Chinnapaiyan S (2018). Microwave-assisted synthesis of Bi_2WO_6 flowers decorated graphene nanoribbon composite for electrocatalytic sensing of hazardous dihydroxybenzene isomers. Composites. Part B, Engineering, 152: 220–230

Ren H, Qi F, Labidi A, Zhao J, Wang H, Xin Y, Luo J, Wang C (2023). Chemically bonded carbon quantum dots/Bi_2WO_6 S-scheme heterojunction for boosted photocatalytic antibiotic degradation: Interfacial engineering and mechanism insight. Applied Catalysis B: Environmental, 330: 122587

Shang Z, Feng X, Chen G, Qin R, Han Y (2023). Recent advances on single-atom catalysts for photocatalytic CO_2 reduction. Small, 19(48): 2304975

Shi Y, Zhao Z, Yang D, Tan J, Xin X, Liu Y, Jiang Z (2023). Engineering photocatalytic ammonia synthesis. Chemical Society Reviews, 52(20): 6938–6956

Song N, Zhang S, Zhong S, Su X, Ma C (2022). A direct Z-scheme polypyrrole/Bi_2WO_6 nanoparticles with boosted photogenerated charge separation for photocatalytic reduction of Cr(VI): characteristics, performance, and mechanisms. Journal of Cleaner Production, 337: 130577

Song J, Li C, Wang X, Zhi S, Wang X, Sun J (2021). Visible-light-driven heterostructured g-C_3N_4/Bi-TiO_2 floating photocatalyst with enhanced charge carrier separation for photocatalytic inactivation of *Microcystis aeruginosa*. Frontiers of Environmental Science & Engineering, 15(6): 129

Tao R, Li X, Li X, Liu S, Shao C, Liu Y (2020). Discrete heterojunction nanofibers of $BiFeO_3$/Bi_2WO_6: novel architecture for effective charge separation and enhanced photocatalytic performance. Journal of Colloid and Interface Science, 572: 257–268

Torres‐Pinto A, Silva C G, Faria J L, Silva A M T (2021). Advances on graphyne-family members for superior photocatalytic behavior. Advanced Science, 8(10): 2003900

Verma A, Dhanaraman E, Chen W T, Fu Y P (2023). Optimization of intercalated 2D BiOCl sheets into Bi_2WO_6 flowers for photocatalytic NH_3 production and antibiotic pollutant degradation. ACS Applied Materials & Interfaces, 15(31): 37540–37553

Wang J, Tang L, Zeng G, Deng Y, Dong H, Liu Y, Wang L, Peng B, Zhang C, Chen F (2018a). 0D/2D interface engineering of carbon quantum dots modified Bi_2WO_6 ultrathin nanosheets with enhanced photoactivity for full spectrum light utilization and mechanism insight. Applied Catalysis B: Environmental, 222: 115–123

Wang J, Zhi D, Zhou H, He X, Zhang D (2018b). Evaluating tetracycline degradation pathway and intermediate toxicity during the electrochemical oxidation over a Ti/Ti_4O_7 anode. Water Research, 137: 324–334

Wang L, Wang Z, Zhang L, Hu C (2018c). Enhanced photoactivity of Bi_2WO_6 by iodide insertion into the interlayer for water purification under visible light. Chemical Engineering Journal, 352: 664–672

Wang M, Zeng S, Woldu A R, Hu L (2022). $BiVO_4$/Bi_2S_3 Z-scheme heterojunction with MnO_x as a cocatalyst for efficient photocatalytic CO_2 conversion to methanol by pure water. Nano Energy, 104: 107925

Wang S, Xiong Z, Yang N, Ding X, Chen H (2020a). Iodine-doping-assisted tunable introduction of oxygen vacancies on bismuth tungstate photocatalysts for highly efficient molecular oxygen activation and pentachlorophenol mineralization. Chinese Journal of Catalysis, 41(10): 1544–1553

Wang T, Bai Y, Si W, Mao W, Gao Y, Liu S (2021a). Heterogeneous photo-Fenton system of novel ternary Bi_2WO_6/$BiFeO_3$/g-C_3N_4 heterojunctions for highly efficient degrading persistent organic pollutants in wastewater. Journal of Photochemistry and Photobiology A Chemistry, 404: 112856

Wang T, Feng C, Liu J, Wang D, Hu H, Hu J, Chen Z, Xue G (2021b). Bi_2WO_6 hollow microspheres with high specific surface area and oxygen vacancies for efficient photocatalysis N_2 fixation. Chemical Engineering Journal, 414: 128827

Wang T, Liu S, Mao W, Bai Y, Chiang K, Shah K, Paz-Ferreiro J (2020b). Novel Bi_2WO_6 loaded N-biochar composites with enhanced photocatalytic degradation of Rhodamine B and Cr(VI). Journal of Hazardous Materials, 389: 121827

Wang T, Mao W, Wu Y, Bai Y, Gao Y, Liu S, Wu H (2019). Heterogeneous photo-Fenton degradation of Rhodamine B dye via a high visible-light responsive Bi_2WO_6 and $BiFeO_3$ heterojunction composites. Journal of Materials Science Materials in Electronics, 30(17): 16452–16462

Wang T, Xiao G, Li C, Zhong S, Zhang F (2015). One-step synthesis of a sulfur doped Bi_2WO_6/Bi_2O_3 composite with enhanced visible-light photocatalytic activity. Materials Letters, 138: 81–84

Wang Y, Dai Z, Wang J, Zhang D, Zhou F, Li J, Huang J (2023a). Scheme-II heterojunction of Bi_2WO_6@Br-COFs hybrid materials for CO_2 photocatalytic reduction. Chemical Engineering Journal, 471: 144559

Wang Y, Hu J, Ge T, Chen F, Lu Y, Chen R, Zhang H, Ye B, Wang S, Zhang Y, et al. (2023b). Gradient cationic vacancies enabling inner-to-outer tandem homojunctions: strong local internal electric field and reformed basic sites boosting CO_2 photoreduction. Advanced Materials, 35(31): 2302538

Wei J, Xia Y, Qayum A, Jiao X, Chen D, Wang T (2020). Unexpected photoinduced room temperature magnetization in Bi_2WO_6 nanosheets. Small, 16(50): 2005704

Wu J, Huang Y, Ye W, Li Y (2017). CO_2 reduction: from the electrochemical to photochemical approach. Advanced Science, 4(11): 1700194

Wu S, Sun J, Li Q, Hood Z D, Yang S, Su T, Peng R, Wu Z, Sun W, Kent P R C, et al. (2020). Effects of surface terminations of 2D Bi_2WO_6 on photocatalytic hydrogen evolution from water splitting. ACS Applied Materials & Interfaces, 12(17): 20067–20074

Xiang Y, Ju P, Wang Y, Sun Y, Zhang D, Yu J (2016). Chemical etching preparation of the Bi_2WO_6/BiOI p-n heterojunction with enhanced photocatalytic antifouling activity under visible light irradiation. Chemical Engineering Journal, 288: 264–275

Xing Z, Hu J, Ma M, Lin H, An Y, Liu Z, Zhang Y, Li J, Yang S (2019). From one to two: *in situ* construction of an ultrathin 2D–2D closely bonded heterojunction from a single-phase monolayer nanosheet. Journal of the American Chemical Society, 141(50): 19715–19727

Xu S, Zhang Y J, Tang R, Zhang X, Hu Z H, Yu H Q (2021). Enhancing Fenton-like catalytic efficiency of Bi_2WO_6 by iodine doping for pollutant degradation. Separation and Purification Technology, 277: 119447

Xu X, Ge Y, Li B, Fan F, Wang F (2014). Shape evolution of Eu-doped Bi_2WO_6 and their photocatalytic properties. Materials Research Bulletin, 59: 329–336

Xue X, Chen X, Zhang Z, Fan G, Ma T (2023). Improved ionic organic pollutant degradation under visible light by Ag SPR-promoted phosphorus-doped g-C_3N_4/AgBr/Bi_2WO_6 with excellent charge transfer capacity and high surface area. Journal of Alloys and Compounds, 930: 167457

Yan T, Yang Q, Feng R, Ren X, Zhao Y, Sun M, Yan L, Wei Q (2022). Highly effective visible-photocatalytic hydrogen evolution and simultaneous organic pollutant degradation over an urchin-like oxygen-doped MoS_2/$ZnIn_2S_4$ composite. Frontiers of Environmental Science & Engineering, 16(10): 131

Yang C, Zhang Z, Wang P, Xu P, Shen T, Wang M, Zheng Q, Zhang G (2023a). Ultrathin g-C_3N_4 composite Bi_2WO_6 embedded in PVDF UF membrane with enhanced permeability, anti-fouling performance and durability for efficient removal of atrazine. Journal of Hazardous Materials, 451: 131154

Yang J, Wang L, Yang J, Li C, Zhong S (2023b). Magnetic biochar coupled with bismuth tungstate for multiple antibiotic removal from contaminated water: characteristics, performance, and competitive adsorption synergistic photocatalysis mechanism. Journal of Environmental Chemical Engineering, 12(1): 111768

Yang M, Xu T, Jin X, Shen Q, Sun C (2022). Oxygen vacancies enriched Bi_2WO_6 for enhanced decabromodiphenyl ether photodegradation via C-Br bond activation. Applied Surface Science, 581(15): 152439

Yang X, Ma Y, Liu Y, Wang K, Wang Y, Liu M, Qiu X, Li W, Li J (2021). Defect-induced Ce-doped Bi_2WO_6 for efficient electrocatalytic N_2 reduction. ACS Applied Materials & Interfaces, 13(17): 19864–19872

Ye K, Li Y, Yang H, Li M, Huang Y, Zhang S, Ji H (2019). An ultrathin carbon layer activated CeO_2 heterojunction nanorods for photocatalytic degradation of organic pollutants. Applied Catalysis B: Environmental, 259: 118085

Yi H, Qin L, Huang D, Zeng G, Lai C, Liu X, Li B, Wang H, Zhou C, Huang F, et al. (2019). Nano-structured bismuth tungstate with controlled morphology: fabrication, modification, environmental application and mechanism insight. Chemical Engineering Journal, 358: 480–496

Yuan T, Li Z, Zhang W, Xue Z, Wang X, Ma Z, Fan Y, Xu J, Wu Y (2019). Highly sensitive ethanol gas sensor based on ultrathin nanosheets assembled Bi_2WO_6 with composite phase. Science Bulletin, 64(9): 595–602

Zeng Y, Yin Q, Liu Z, Dong H (2022). Attapulgite-interpenetrated g-C_3N_4/Bi_2WO_6 quantum-dots Z-scheme heterojunction for 2-mercaptobenzothiazole degradation with mechanism insight. Chemical Engineering Journal, 435: 134918

Zhang C, Ren J, Hua J, Xia L, He J, Huo D, Hu Y (2018a). Multifunctional Bi_2WO_6 nanoparticles for CT-guided photothermal and oxygen-free photodynamic therapy. ACS Applied Materials & Interfaces, 10(1): 1132–1146

Zhang C, Xia D, Liu J, Huo D, Jiang X, Hu Y (2020a). Bypassing the immunosuppression of myeloid-derived suppressor cells by reversing tumor hypoxia using a platelet-inspired platform. Advanced Functional Materials, 30(22): 2000189

Zhang J, Yuan X, Jiang L, Wu Z, Chen X, Wang H, Wang H, Zeng G (2018b). Highly efficient photocatalysis toward tetracycline of nitrogen doped carbon quantum dots sensitized bismuth tungstate based on interfacial charge transfer. Journal of Colloid and Interface Science, 511: 296–306

Zhang L, He F, Mao W, Guan Y (2020b). Fast and efficient removal of Cr(VI) to ppb level together with Cr(III) sequestration in water using layered double hydroxide interclated with diethyldithiocarbamate. Science of the Total Environment, 727: 138701

Zhang L, Yang C, Lv K, Lu Y, Li Q, Wu X, Li Y, Li X, Fan J, Li M (2019). SPR effect of bismuth enhanced visible photoreactivity of Bi_2WO_6 for NO abatement. Chinese Journal of Catalysis, 40(5): 755–764

Zhang M, Mao Y, Bao X, Zhai G, Xiao D, Liu D, Wang P, Cheng H, Liu Y, Zheng Z, et al. (2023). Coupling benzylamine oxidation with CO_2 photoconversion to ethanol over a black phosphorus and bismuth tungstate S-scheme heterojunction. Angewandte Chemie International Edition, 62(36): e202302919

Zhang X, Han F, Shi B, Farsinezhad S, Dechaine G P, Shankar K (2012). Photocatalytic conversion of diluted CO_2 into light hydrocarbons using periodically modulated multiwalled nanotube arrays. Angewandte Chemie International Edition, 51(51): 12732–12735

Zhang Y, Li Y, Yuan Y (2022). Carbon quantum dot-decorated BiOBr/Bi_2WO_6 photocatalytic micromotor for environmental remediation and DFT calculation. ACS Catalysis, 12(22): 13897–13909

Zhang Z, Wang W, Gao E, Shang M, Xu J (2011). Enhanced photocatalytic activity of Bi_2WO_6 with oxygen vacancies by zirconium doping. Journal of Hazardous Materials, 196: 255–262

Zhao S, Chen C, Ding J, Yang S, Zang Y, Ren N (2022). One-pot hydrothermal fabrication of $BiVO_4$/Fe_3O_4/rGO composite photocatalyst for the simulated solar light-driven degradation of Rhodamine B. Frontiers of Environmental Science & Engineering, 16(3): 36

Zhao L, Hou H, Wang L, Bowen C R, Wang J, Yan R, Zhan X, Yang H, Yang M, Yang W (2024a). Atomic-level surface modification of ultrathin Bi_2WO_6 nanosheets for boosting photocatalytic CO_2 reduction. Chemical Engineering Journal, 480: 148033

Zhao L, Wang J, Yang W, Hou H, Yan R (2023). Efficient photoreduction of carbon dioxide into carbon-based fuels: a review. Environmental Chemistry Letters, 21(3): 1499–1513

Zhao Y, Fan X, Zheng H, Liu E, Fan J, Wang X (2024b). $Bi_2WO_6/AgInS_2$ S-scheme heterojunction: efficient photodegradation of organic pollutant and toxicity evaluation. Journal of Materials Science and Technology, 170: 200–211

Zhao Y, Liang X, Wang Y, Shi H, Liu E, Fan J, Hu X (2018a). Degradation and removal of *Ceftriaxone sodium* in aquatic environment with Bi_2WO_6/g-C_3N_4 photocatalyst. Journal of Colloid and Interface Science, 523: 7–17

Zhao Y, Wang Y, Liu E, Fan J, Hu X (2018b). Bi_2WO_6 nanoflowers: an efficient visible light photocatalytic activity for ceftriaxone sodium degradation. Applied Surface Science, 436: 854–864

Zheng X, Han T, Shi H (2023). Cu-doped Bi_2WO_{6-x} photocatalyst with efficient charge separation ability for enhanced peroxymonosulfate activation. Journal of Molecular Liquids, 391: 123273

Zhou F, Zhu Y (2012). Significant photocatalytic enhancement in methylene blue degradation of Bi_2WO_6 photocatalysts via graphene hybridization. Journal of Advanced Ceramics, 1(1): 72–78

Zhou Y, Zhang Y, Lin M, Long J, Zhang Z, Lin H, Wu J C S, Wang X (2015). Monolayered Bi_2WO_6 nanosheets mimicking heterojunction interface with open surfaces for photocatalysis. Nature Communications, 6(1): 8340